A simple analytical approximation to the temperature structure in subduction zones

Philip England[1] and Catherine Wilkins[2]

[1]*Department of Earth Sciences, Oxford University, Parks Road, Oxford* OX1 3PR, *UK. E-mail: philip.england@earth.ox.ac.uk*
[2]*St Hugh's College, Oxford* OX2 6LE, *UK*

SUMMARY
A simple model is employed to find scaling relations between key features of the temperature structure of subduction zones and subduction zone parameters. Flow in the wedge of mantle between the slab and the overriding plate is approximated by the corner flow of a Newtonian viscous fluid. The flow maintains an advective boundary layer on top of the slab that controls the temperature at the interface between the slab and the wedge. This temperature, the maximum temperature in the wedge above the slab, and the thickness of the advective boundary layer, all depend on a single dimensionless distance, $Vr\delta^2/\kappa$, where V is the speed of plate convergence, r is distance from the corner of the wedge, δ is the dip of the slab and κ is thermal diffusivity. The observation that volcanic fronts at island arcs lie above places where the slab reaches a depth that correlates negatively with convergence rate and slab dip suggests that the thermal structure of subduction zones may be described by the simple scaling developed here, and that the locations of the arcs are controlled by a strongly temperature-dependent process taking place in the wedge.

Key words: island arcs, subduction zones, thermal structure, volcanoes.

1 INTRODUCTION

The recent observation (England *et al.* 2004) that the depth of the top of the intermediate-depth seismicity beneath arc volcanoes (interpreted as lying close to the top of the slab) varies systematically with the speed of descent of the slab has motivated us to seek scaling relations for temperatures in subduction zones in order to develop understanding of this systematic variation, and to provide a simple framework in which to investigate its implications for the processes of melting and melt transport in subduction zones.

We simplify the problem as far as possible by assuming that the wedge of mantle between a slab and an overriding plate is a Newtonian fluid, whose motion is driven entirely by the relative motion of its bounding plates (see Fig. 1, Section 2). The main mathematical development of the paper is contained in the Appendix, in which we derive approximate expressions for the temperatures along the top of a slab and in the wedge of mantle above the it. We show that these approximations depend on a single parameter—a dimensionless distance $r' = Vr\delta^2/\kappa$, where V is convergence rate, δ is dip of the slab, κ is thermal diffusivity and r is distance from the wedge corner. We compare, in Section 3, the temperatures predicted by the simple scaling relations with numerical calculations, and show that over the full range of parameters pertaining to active subduction zones the scaling derived from our analytical approximations is in agreement with numerical solutions to the full equations. Section 4 uses the scaling relations along with the observed systematics in the distribution of volcanoes (England *et al.* 2004) to draw inferences about the processes controlling the location of arc volcanoes.

2 THE MATHEMATICAL MODEL

The configuration we assume for the motion of material in subduction zones is shown in Fig. 1. The overriding plate is taken to be fixed; the subducting plate has thickness a, converges with the overriding plate at speed V and descends into the mantle with a dip δ. (The notation we use is given in Table 1.) The relative motion between the two plates drives flow in the wedge of mantle between them. Similarly, the subducting plate drives a flow in the obtuse wedge beneath it. In this section we define our mathematical model by prescribing the form of these flows, and giving the boundary conditions on temperature. The main aim of this paper is to use a simplified model to determine scaling relations for the temperature in subduction zones; because these expressions are tested against full (numerical) solutions to the model, we outline in this section the numerical techniques employed.

2.1 The velocity field

The wedges of mantle above and below the subducting plate are treated as incompressible Newtonian fluids of essentially infinite extent (Fig. 1). This assumption allows us to use 'corner flow' solutions of simple analytical form for the flow (Batchelor 1967; McKenzie 1969).

The velocity in the wedge, $\mathbf{u}(u_r, u_\theta)$, can be expressed in terms of a stream function, ψ:

$$u_r = \frac{1}{r}\frac{\partial\psi}{\partial\theta} \tag{1}$$
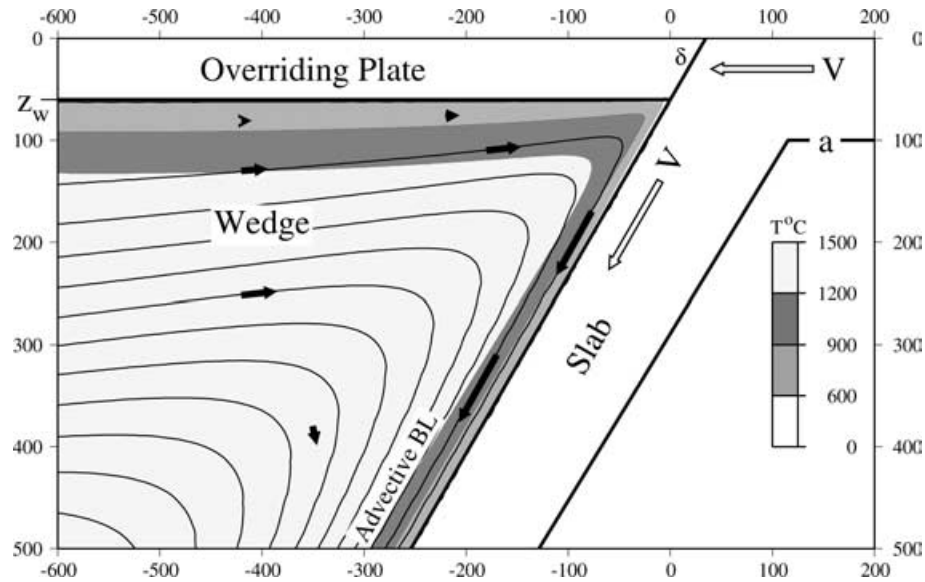
Figure 1. Idealized sketch of a subduction zone, illustrating terminology and parameters used in the paper. Two plates converge at a speed V, measured perpendicular to the trend of the island arc. A slab, of thickness a, dips at an angle, δ, beneath the overriding plate. The relative motion between the slab and overriding plate generates circulation in the wedge of mantle between them, which is here depicted as conforming to the flow of a Newtonian fluid with velocity equal to zero on the top of the wedge and equal to the velocity of the slab on the base of the wedge (the corner flow of McKenzie 1969). The base of the overriding plate, and thus the wedge corner, are at depth z_w, and the boundary between the two plates lies on the top of the slab, from the surface to the wedge corner at depth z_w. The material of the wedge follows stream lines, shown as curved lines; illustrative arrows show the relative magnitudes of the velocity in different parts of the wedge. Shading depicts the portion of the wedge that is cooler than the background temperature of the mantle, T_a, while still being hot enough to participate in the flow. This layer forms an insulating boundary on the top of the subducting slab.

$$u_\theta = -\frac{\partial \psi}{\partial r} \tag{2}$$

where r, θ are polar coordinates whose origin is at the corner of the flow (Batchelor 1967).

The stream function for the corner flow beneath the subducting plate is (McKenzie 1969):

$$\psi = \frac{r V[(\theta - \omega)\sin\theta - \theta\sin(\theta - \omega)]}{\omega + \sin\omega} \tag{3}$$

where δ is the dip of the slab, $\omega = \pi - \delta$ and θ is measured clockwise from the horizontal base of the subducting plate. This expression is used only when we solve numerically for the temperatures in slab and mantle. In practice, the details of this flow are unimportant for the region of interest, which is the top of the slab and its overlying wedge of mantle, because the timescale for thermal diffusion through the slab, $\sim a^2/\pi^2\kappa$, greatly exceeds the timescale for advection of heat in the wedge (see Section A3).

We take the velocity of the descending slab to be parallel to the slab. With the overriding plate having zero velocity, the stream function, ψ, for the flow in the wedge above the slab is given by (McKenzie 1969):

$$\psi = \frac{r V [(\delta - \theta)\sin\theta\sin\delta - \delta\theta\sin(\delta - \theta)]}{\delta^2 - \sin^2\delta} \tag{4}$$

where θ is measured counter-clockwise from the horizontal base of the overriding plate (Fig. 1).

We also investigate the case in which free slip is allowed at the base of the overriding plate, for which the solution is:

$$\psi = \frac{r V [\delta\cos\delta\sin\theta - \theta\sin\delta\cos\theta]}{\delta - \cos\delta\sin\delta}. \tag{5}$$

It is worth noting, for completeness, that a condition of free slip on the top of the slab would result in a static wedge; this case has

been treated by Molnar & England (1990), but is of no interest in the current context because temperatures in such a static wedge would never be high enough to yield melting beneath the island arcs.

2.2 Thermal model

In both numerical and analytical solutions, we take the temperature at the surface of the Earth to be zero (and 0 °C when dimensional quantities are used). The temperatures on the side boundaries are taken to be

$$T = \frac{T_a z}{a} \qquad z \leq a \tag{6}$$

$$T = T_a \qquad z > a \tag{7}$$

$$T = \frac{T_a z}{z_w} \qquad z \leq z_w \tag{8}$$

$$T = T_a \qquad z > z_w \tag{9}$$

where z is depth beneath the Earth's surface, and T_a is the background temperature of the upper mantle. Eqs (6) and (7) refer to the right-hand side and (8) and (9) refer to the left-hand side beneath the overriding plate. We do not use the error function or Fourier series solution for the temperature structure of the oceanic lithosphere because temperature variations due to differences in thickness, a, of the plate are much more important than details of the temperature structure within a plate of a given thickness.

In the numerical calculations, the base of the zone of calculation is at a depth of 800 km; the right-hand boundary is 500 km to the right of the trench, and the left-hand boundary is taken to be 1500 km to the left of the slab at the base of the solution domain. We assume zero vertical derivative of temperature on the base of the solution domain.

Table 1. Notation, with expressions for, or values of, parameters.

Symbol	Definition	Notation/value
a	Thickness of the slab	40–100 km
c	Specific heat	10^3 J kg^{-1} K^{-1}
K	Thermal conductivity	$\kappa\,\rho\,c$
R	Scale length for temperature change in wedge	$400\,\kappa/V\delta^2$
r	Radial distance from wedge corner	
r'	Dimensionless radial distance from wedge corner	$Vr\delta^2/\kappa$
T	Temperature	
T_a	Background temperature of the upper mantle	1280 °C
T_s	Temperature at the top surface of the slab	$\left[T_1 + \frac{\pi\alpha T_a}{2a}\operatorname{erf}(\frac{a}{2\sqrt{\kappa t}})\right]\left(1 + \frac{\sqrt{\pi}\alpha}{2\beta}\right)^{-1}$
T_1	Maximum temperature in the wedge on a	$T_a\exp\left\{\frac{1}{2}\left[1 - \left(\frac{R}{r}\right)^{1/3}\right]\right\}$ $0 < r < R$
	profile perpendicular to the slab	T_a $r \geq R$
u_x	Component of velocity in the wedge perpendicular to the slab	
U_x	Maximum value of u_x on a profile perpendicular to the slab	
V	Convergence rate between plates	
x	Distance measured perpendicular to the top of the slab	
z	Depth below Earth's surface	
z_w	Depth of wedge corner, equal to thickness of the overriding plate	40, 60, 80 km
α	Thickness of advective boundary layer on top of slab	$r\delta(16/9\sqrt{\pi}\xi r')^{1/3}$
β	Thickness of inverted thermal gradient within slab	$\sqrt{\kappa z/(V\sin\delta)}$
δ	Dip of the slab	
κ	Thermal diffusivity	8×10^{-7} m^2 s^{-1}
θ	Angle within wedge, measured from horizontal	
ξ		$1 - \frac{2}{5}\sec(2\delta/5)$
ρ	Density	3300 kg m^{-3}
ϕ	Angle within wedge, measured from slab	$\delta - \theta$
ψ	Stream function for flow in wedge	

Dissipative heating is neglected throughout; we discuss this assumption further below (Section 3.4.2). We also assume that heat transfer is by advection and diffusion through the solid wedge and plates, ignoring transport of heat and mass by flow through connected porosity or cracks. Finally, we assume thermal steady state and solve the time-independent advection–diffusion equation for temperature, T, in an incompressible medium of constant thermal diffusivity, κ:

$$\mathbf{v}\cdot\nabla T = \kappa\nabla^2 T, \tag{10}$$

where $\mathbf{v}$ is the velocity of the medium.

2.3 Numerical solution

We calculate numerical solutions to (10) by the finite-element method, using the streamline upwind Petrov–Galerkin method (e.g. Johnson 1990). We employ grids that are greatly densified close to the wedge corner, in the boundary layers at the top of the slab and at the bases of the slab and plates, typically with around 10^5 nodes and 2×10^5 elements. We have tested for convergence, and find that solutions obtained with these meshes agree to within 1 per cent with those obtained with twice the mesh spacing. We assessed the accuracy of our solutions by computing numerical solutions to the problem considered by Molnar & England (1990) in which a rigid slab moves beneath a stationary wedge. Although that problem does

not contain relative motion within the wedge, which is an important part of the present problem, it does contain, at the top of the slab, thermal gradients that are as steep as those encountered here. Molnar & England (1990) give approximate analytical expressions for the temperature in the wedge and on the top of the slab, obtained by ignoring thermal diffusion parallel to the slab. We find that, for $\delta < 20°$ and 30 mm yr^{-1} $< V <$ 150 mm yr^{-1}, our solutions agree with these analytical solutions to within 2 per cent, consistent with the degree of approximation in the expressions of Molnar & England (1990).

To evaluate the validity of the scaling relations derived in this paper, we obtain numerical solutions for slab dips of 10° to 80°, in steps of 10°, for convergence speeds of 10 to 100 mm yr^{-1}, in steps of 10 mm yr^{-1}. We show the results from two suites of calculations; in the first the thickness, a, of the slab is 100 km and depths to the wedge corner, z_w, are 40, 60 or 80 km. In the second suite, z_w is fixed at 60 km, and a is taken to be 40, 60 or 80 km.

3 APPROXIMATE ANALYTICAL EXPRESSIONS

Although our analytical approximations are independent of the numerical solutions with which we check them, it is useful to begin our discussion with an illustrative calculation that displays the principal features of the problem. We are concerned with the temperature in

three parts of the system: the overriding plate, whose base is defined by the constant depth, z_w; the slab, whose top is defined by a plane of constant dip, δ, and the wedge of fluid mantle between these rigid layers. (As discussed above, the temperature field below the subducting plate does not influence significantly the temperatures in the rest of the system.)

Fig. 1 shows a portion of the solution domain for a calculation in which the thickness of the overriding pate, z_w, is 60 km, the slab thickness, a, is 100 km, the dip, δ, of the slab is 60° and the plate convergence rate is 100 mm yr^{-1}. There are two parts of the wedge in which the thermal gradient is appreciably steeper than in the interior of the wedge. The first of these is the boundary layer beneath the overriding plate, where the upward component of the corner flow carries heat to the base of the plate. The second part lies immediately above the slab, where the corner flow carries heat downwards to the top of the slab. The key to our analytical expressions lies in the temperature structure of this advective boundary layer on top of the slab. This layer partly insulates the slab from the mantle wedge and our solution therefore differs significantly from that of McKenzie (1969), which treats the mantle outside the slab as being isothermal and applying a constant, high, temperature on the top of the slab.

3.1 Thickness of the advective boundary layer on top of the slab

The boundary layer beneath the overriding plate layer thins as it is advected towards the slab; in the particular illustration of Fig. 1, the layer of steep thermal gradient on top of the slab has approximately one-quarter of the thickness of the equivalent layer beneath the overriding plate. Davies & Stevenson (1992) obtained an analytical solution for the temperature structure in the advective boundary layer on top of the slab, under the assumption that it has a constant thickness of a few kilometres. This assumption is retained by Davies (1999) in his analytical solution to the problem but, because the thickness of the advective boundary layer on top of the slab depends upon the speed of the flow in the wedge, Davies' solution is incomplete.

In the Appendix we show that, in the corner flow, the maximum value of the component of velocity in the wedge perpendicular to the slab is $\sim V\delta/4$, where V is the speed of convergence between the plates and δ is the dip of the slab (see Table 1 for notation). Assuming that diffusion of heat parallel to the slab is negligible in comparison with diffusion and advection of heat perpendicular to the slab, we show that the thickness, α, of the advective boundary layer on top of the slab is

$$\alpha \sim \left(\frac{16\kappa r^2\delta}{9\sqrt{\pi}\xi V}\right)^{1/3} = r\delta\left(\frac{16}{9\sqrt{\pi}\xi r'}\right)^{1/3}. \tag{11}$$

In this expression, r is distance from the wedge corner, ξ is a factor dependent weakly on the dip of the slab (see eq. A4) that is close to 0.6, and r' is a dimensionless distance, given by

$$r' = \frac{Vr\delta^2}{\kappa}.$$

The form of the expression for the thickness of the thermal boundary layer arises from the balance between diffusion and advection of heat, which is often expressed in terms of the Péclet number, or thermal Reynolds number. The Péclet number is the ratio of the length of time required for heat to diffuse through a layer of a given thickness to the length of time taken for heat to be carried the same distance by the flow. For a boundary layer of thickness α, these times are approximately equal to $\alpha^2/(\pi^2\kappa)$ and α/U, respectively, where

U is the characteristic speed of the flow in the boundary layer. Section A2 shows that, at the top of the boundary layer, material moves towards the slab at a rate $U \sim 9\pi^2\,V\xi\alpha^2/16\,r^2\delta$ (series substitution for cosine in eq. A9). The thickness of the advective boundary layer is determined by the requirement that its diffusional and advective timescales be comparable:

$$\frac{U}{\alpha}\frac{\alpha^2}{\pi^2\kappa} = \frac{9V\xi\alpha^3}{16\kappa r^2\delta} \sim 1, \tag{12}$$

which gives an approximate expression for α:

$$\alpha \approx \left(\frac{16\kappa r^2\delta}{9V\xi}\right)^{1/3} \tag{13}$$

that closely resembles (11).

The temperature in the advective boundary layer on top of the slab is given by

$$T(x) = T_s + (T_1 - T_s)\mathrm{erf}\left(\frac{x}{\alpha}\right), \tag{14}$$

where T_s is the temperature on the top of the slab at a distance r from the wedge corner, and T_1 is the maximum temperature in the wedge on a profile perpendicular to the slab, starting at the same distance, r, from the wedge corner (see eq. A18), and x is distance along that profile. (Expressions for T_s and T_1 are given below.)

We evaluate the accuracy of the expression for α using our numerical solutions. For each calculation we take temperature profiles perpendicular to the slab at integer multiples of 25 km, starting below z_w and continuing to 300 km. We then fit an error function solution to each profile to obtain the best-fitting value of α. We find that (11) gives an accurate estimate of the thickness of the boundary layer on top of the slab, provided that $\alpha < \pi\sqrt{\kappa t}$ where $t = r/V$ is the length of time that the top of the slab has been in contact with the wedge. We may expect a breakdown in the assumptions that led to (11) when the length scale associated with thermal diffusion, proportional to $\sqrt{\kappa t}$, becomes comparable with the thickness of the advective boundary layer on top of the slab . If we modify (11), by setting the boundary layer thickness to be the smaller of α and $\pi\sqrt{\kappa t}$, then we have an accurate description of the boundary layer thickness for almost the full range of parameters we investigate (Fig. 2).

We exclude from Fig. 2 those calculations for which $t > a^2/\pi^2\kappa$. In these cases, the timescale for diffusion of heat through the slab is less than the length of time that the top of the slab has been in contact with the wedge, so the heat flux from within the slab varies significantly with distance along the slab, rendering invalid the assumption that we can neglect diffusion parallel to the slab.

3.2 Maximum temperature in the wedge

The remaining parameter required for the description of temperatures in the wedge is T_1, the maximum temperature in the wedge along a profile taken perpendicular to the slab. Eq. (14) shows that, along any profile perpendicular to the top of the slab, temperatures rise from T_s, the temperature at the top of the slab, to T_1 over a distance $\sim\alpha$, given by (11). Temperatures in the interior of the wedge are thereafter isothermal, until the thermal boundary layer at the base of the overriding plate is reached. Further, as we show below, the temperature on the top of the slab is, itself, determined by T_1.

We obtain an expression for T_1 by considering the heat balance in the wedge (see Section A4). As for the thermal boundary layer on top of the slab (see Section A2.1), this balance is between thermal diffusion and advection of heat by the flow. Whereas the characteristic speed within the advective boundary layer on top of the slab is
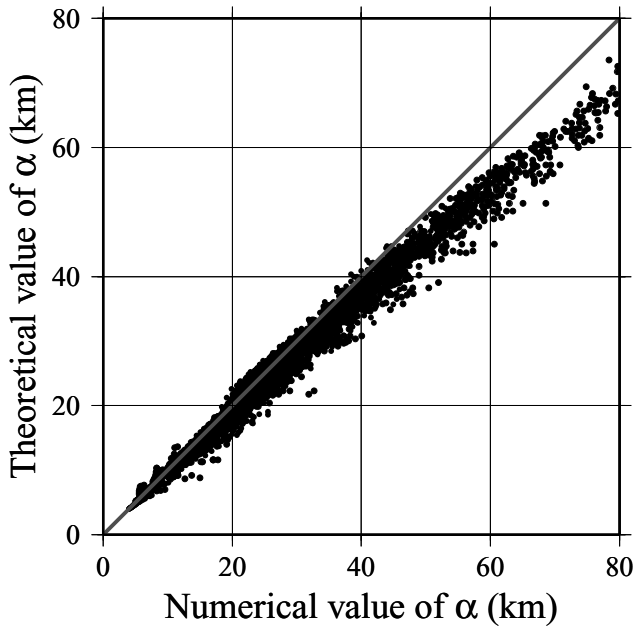
Figure 2. Comparison between the theoretical expression for the thickness, α (see eqs 11 and A17) of the advective boundary layer on top of the slab and the thickness determined from numerical solutions (see text). The theoretical expression for the thickness of the advective boundary layer on top of the slab is given by the smaller of α (eq. 11) and $\pi\sqrt{\kappa t}$, where $t = r/V$ is the length of time for which the top of the slab has been in contact with the wedge (solid symbols). Numerical solutions are obtained for slab dips between 10° and 80°, and for convergence speeds between 10 and 100 mm yr^{-1}. Calculations are shown for two combinations of the thickness, a, of the slab and z_w, the depth to the wedge corner: z_w is fixed to 60 km, with a being 40, 60 or 80 km, or a is fixed to 100 km, with z_w being 40, 60 or 80 km. Solutions are not plotted in the cases where the speed of descent was so slow that no error function could be fit to the profile (usually $V \sin\delta < 10$ mm yr^{-1}), or when heat flux from within the slab varies appreciably with distance along the slab ($t > a^2/\pi^2\kappa$).

generally a small fraction of the convergence rate, V, heat is carried within the wedge at a speed comparable to V. Heat is carried both downwards, by cold material in the slab and the fluid it entrains, and upwards by rising hot material of the wedge; the combined effect is to advect heat towards the wedge corner. This advection is balanced by the diffusion of heat out of the wedge into the surrounding plates. Our simple analysis neglects the diffusion through the over-riding plate and concentrates on the much steeper thermal gradient through the advective boundary layer on top of the slab , and we find (see eqs A38–A47)

$$T_1 \sim T_a \exp\left\{\frac{1}{2}\left[1 - \left(\frac{R}{r}\right)^{1/3}\right]\right\} \qquad 0 < r < R$$
$$T_1 = T_a \qquad\qquad\qquad\qquad\qquad r \geq R, \tag{15}$$

where R is a length scale, given by

$$R \sim \frac{400\kappa}{V\delta^2}. \tag{16}$$

We evaluate the validity of our approximation for T_1 from the numerical solutions. The maximum temperature in the wedge, T_1, is plotted against its theoretical value, given by (A47), in Fig. 3. For all cases, the misfit between the approximate expression for T_1 and the numerical value is less than about 100 °C; the r.m.s. misfit is 50 °C, which is equivalent to 5–10 per cent of the magnitude of T_1.
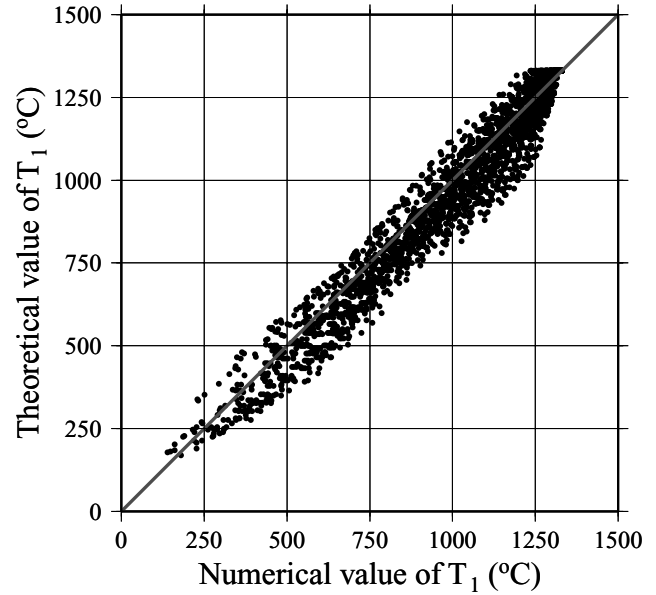
Figure 3. Comparison between theoretical and numerical values of maximum temperature, T_1, in the wedge at different distances from the wedge corner. Numerical solutions are obtained for slab dips between 10° and 80°, and for convergence speeds between 10 and 100 mm yr^{-1}. Calculations are shown for two combinations of the thickness, a, of the slab and z_w, the depth to the wedge corner: z_w is fixed to 60 km, with a being 40, 60 or 80 km, or a is fixed to 100 km, with z_w being 40, 60 or 80 km. Theoretical values for T_1 are calculated from (15).
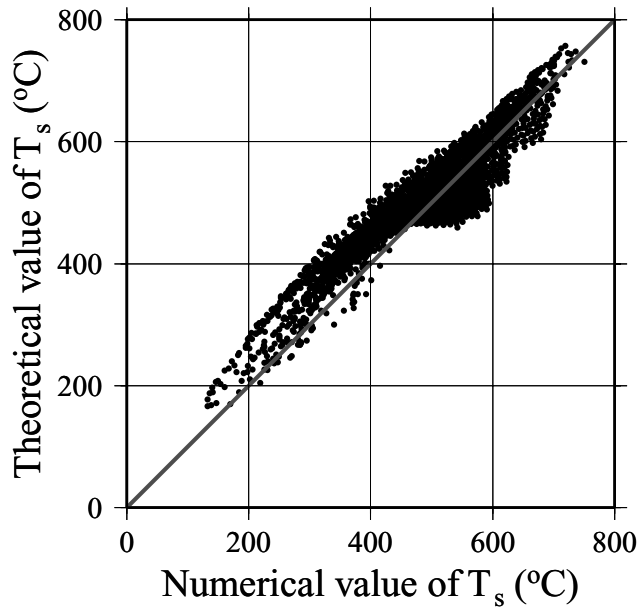
3.3 Temperature at the top of the slab

The temperature gradient at the top of the slab is approximately T_s/β, where the length scale, $\beta = \sqrt{\kappa t}$ is set by the time, t, taken for the top of the slab to reach the depth of interest. The temperature gradient at the bottom of the advective boundary layer on top of the slab is approximately T_s/α, where α is the thickness of the boundary layer. The requirement that these two gradients be equal, to conserve heat flux, gives an expression for the temperature on the top of the slab in terms of the maximum temperature in the wedge above it (see eqs A25–A35):

$$T_s \sim \left[T_1 + \frac{\sqrt{\pi}\alpha T_a}{2a}\mathrm{erf}\left(\frac{a}{2\sqrt{\kappa r/V}}\right)\right]\bigg/\left(1 + \frac{\sqrt{\pi}\alpha}{2\beta}\right) \tag{17}$$

where T_1 is the maximum temperature in the wedge along the profile taken perpendicular to the slab, T_a is the background temperature of the mantle and a is the thickness of the slab.

We evaluate the validity of (17) from our numerical solutions. Fig. 4 shows the value of T_s, calculated from (17) with T_1 given by (15), plotted against the numerical solution for temperature at the top of the slab for each profile. For all cases in which the speed of descent of the slab, $V \sin\delta$, is greater than 10 mm yr^{-1}, the misfit between the approximate expression for T_s and the numerical value is less than about 100 °C. More importantly, for our purpose, Fig. 4 shows that the numerical values for T_s follow the scaling of (17).

Fig. 5 shows that temperatures on the top of the slab (at depths shallower than 300 km) do not rise above about 600 °C unless the thickness of the slab is less than about 40 km. Furthermore, the temperatures on the top of the slab appear to be insensitive to the convergence rate, and to the dip of the slab. This behaviour, which

Figure 4. Comparison between theoretical and numerical values of temperature, T_s, at the top of the slab. The ranges of parameters for the numerical solutions are given in the caption to Fig. 2. Calculations are for the range of conditions given in the caption to Fig. 3.

has been noted by others previously (e.g. Davies & Stevenson 1992; Peacock *et al.* 1994), arises from the thermal boundary condition at the interface between the slab and the wedge.

For slabs older than about 50 Myr, $\alpha \ll a$ so we may neglect the second term in the numerator of (17) and the expression for the temperature at the top of the slab becomes

$$T_s \sim \left(\frac{T_1}{1 + \sqrt{\pi}\alpha/2\beta} \right). \tag{18}$$

The denominator in (18) depends only upon the ratio of the two length scales, α and β, which may be written (see A37) as

$$\frac{\alpha}{\beta} \propto \left(1 - \frac{z_w}{z} \right)\left(\frac{V\delta^2 r}{\kappa} \right)^{1/6}, \tag{19}$$

where z is depth and z_w is depth of the wedge corner. This equation shows that the ratio of the temperature on the top of the slab to the maximum temperature in the wedge above it should depend only weakly on convergence rate (weaker than one-sixth power) and dip (weaker than one-third power) of the subduction zone. Equally, within an individual subduction zone, with V and δ fixed, T_s/T_1 should vary weakly with distance from the wedge corner, for $z \gtrsim z_w$. The appendix (Section A3) shows that α/β ranges from about 1.6 to 2.6 for the range of conditions pertaining to active subduction. Thus we should expect that in the upper few hundred kilometres of subduction zones containing slab of age 50 Myr or older (for which eq. 18 applies), the temperature at the top of the slab would vary only slowly with depth and would not vary greatly, at a given depth, from one subduction zone to another.

3.4 Sensitivity of scaling to model assumptions

The previous sections show that the scaling relations for boundary layer thickness and temperatures agree with the results of full, 2-D, numerical solutions to the steady-state diffusion–advection equation for the model we have adopted. It is appropriate, however, to ask how

sensitive these scalings might be to assumptions made in developing the model.

3.4.1 Assumptions about flow in the wedge

The key to our scaling is the thickness, α, of the advective boundary layer on top of the slab. This parameter appears both in the expression for T_1, the maximum temperature in the wedge interior, and in the relation between T_1 and T_s, the temperature on the top of the slab. Because the thickness of the advective boundary layer on top of the slab depends directly upon the speed at which the flow in the wedge advects heat towards the slab (Section A2), the scaling developed here depends most directly upon assumptions made about the form of the flow in mantle at subduction zones.

One major geometrical assumption that we make is that the flow in the wedge is directly coupled to the overlying plate; thus the velocity in the wedge is zero at its top (Fig. 1). It has often been suggested, however, that the mantle immediately beneath the lithosphere may be a zone of low viscosity, which could decouple the overriding plate from the wedge (e.g. Mitrovica & Forte 1997). We therefore investigated the thermal structure associated with a wedge having zero shear stress at the base of the overriding plate (eqs A19–A21). The scaling is identical to that discussed above, with the exception that α is about 10 per cent greater than in the no-slip case discussed above. The numerical solutions verify this scaling (Fig. 6), thus we may apply the scaling discussed above to the case of free slip at the top of the wedge by making the appropriate small adjustment to α.

In Section A2.1 we argue that, provided the maximum temperature occurs at a roughly constant angle within the wedge, and the maximum speed of circulation perpendicular to the slab scales with the convergence rate between the plates, then the thickness, α, of the advective boundary layer on top of the slab will still scale with r and r', in a fashion similar to that discussed here. We therefore expect that flow in a wedge of power-law fluid, as investigated by Tovish *et al.* (1978), would yield a scaling similar to that discussed here, though we have not investigated this point.

There are forms of the flow for which the scaling proposed here would definitively be inappropriate. One such form would arise if buoyancy were to play an important role in transporting heat within the wedge. The advection of heat that we consider here is entirely by forced convection, with the velocity scale imposed by the convergence speed of the two plates. The scaling would not, presumably, be perturbed significantly by the migration of small fractions of melt through connected porosity, but it would be inapplicable if free convection of the bulk of the wedge were to occur.

Our analysis is also inapplicable to subduction zones in which significant back-arc spreading takes place. The scalings for the quantities of interest, α, T_1 and T_s, are based on the direct link between the convergence rate, V, and advection of heat towards the wedge corner and towards the top of the slab. When back-arc spreading occurs, this link is broken; the circulation is split (Ribe 1989), with some of the flow being directed towards the wedge corner and some towards the spreading centre. In addition, the flow in the presence of back-arc spreading is intrinsically time dependent and generally short-lived. We have not investigated this problem.

A major simplification in our model is the assumption that the mantle wedge has a constant viscosity. It is seems likely that the large lateral variations in temperature and fluid content of the wedge may generate significant variations in viscosity, and the few numerical experiments that have been carried out with temperature-dependent rheologies (e.g. Furukawa 1993; van Keken *et al.* 2002) show that higher wedge temperatures are obtained than in constant-viscosity
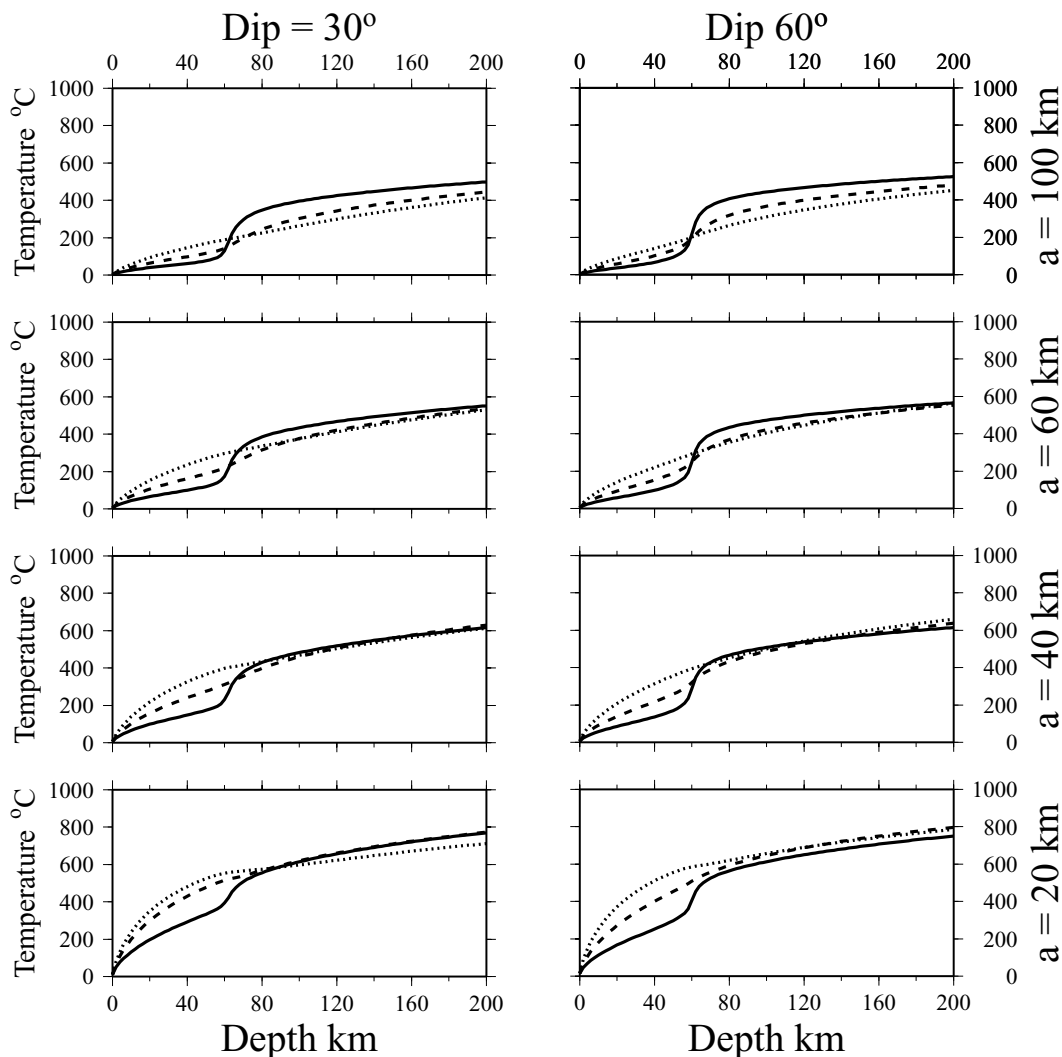
Figure 5. Profiles of temperature along the top of the slab for $\delta = 30°$, $60°$ and $a = 20, 40, 60$ *and* 100 km, with $z_w = 60$ km. Dotted curves illustrate the temperatures for $V = 10$ mm yr^{-1}, dashed curves for $V = 30$ mm yr^{-1} and solid curves for $V = 100$ mm yr^{-1}.

calculations. It remains to be determined whether a scaling comparable to that developed here can be found for flows with temperature-dependent rheology.

3.4.2 Influence of dissipation

We have, so far, neglected dissipation of heat. This approximation is probably valid within the wedge, because McKenzie (1969) shows that typical rates of viscous dissipation are lower than heat generation in mantle rocks if the mantle viscosity is lower than about 10^{21} Pa s. Viscous dissipation on the plate boundary probably is required, however, both to account for the metamorphic conditions recorded by rocks that are believed to have been subducted along plate boundaries (e.g. Peacock 1992) and to explain the heat flux observations near trenches (e.g. Molnar & England 1990; England & Molnar 1991; Von Herzen *et al.* 2001). These studies suggest that stresses of a few tens of MPa may act to depths of about 50 km on subduction zones. Assuming a deviatoric stress of 30 MPa, a dip of $10°$ and a slip rate of 100 mm yr^{-1} yields an estimate of 3×10^4 W m^{-1} for the contribution of dissipation in the upper 50 km to the thermal budget of a subduction zone. An independent estimate of

the total rate of dissipation comes from McKenzie & Jarvis (1980) who used the result that about 2.5 per cent of energy in a convecting system is available to carry out mechanical work on horizontal planes (Jarvis & McKenzie 1980). For a heat flow of 3.4×10^{13} W from the mantle, this yields an estimate of 2×10^4 W m^{-1} for the dissipation on 50 000 km of convergent plate boundary.

As we show above, temperatures in the wedge and at the top of the slab are determined by the advection of heat towards the top of the slab by flow in the wedge. This advection produces boundary layers 10–20 km thick, across which the temperature contrast is more than 600 °C, which is equivalent to a heat flux of ~0.1–0.2 W m^{-2}. Thus the transfer of heat to the top of the slab by dissipation may be comparable with that due to advection in the top 100–200 km of the subduction zone.

We have no analytical solution to offer, but investigate this question further by numerical experiment. In the absence of reliable information on the rates of shear heating on subduction plate boundaries, and in the presence of many competing models for how such heating should be treated, we adopt a simple approach that fixes the temperature on the plate boundary to be the depth multiplied by 10 °C km^{-1}, down to the base of the plate boundary at depth
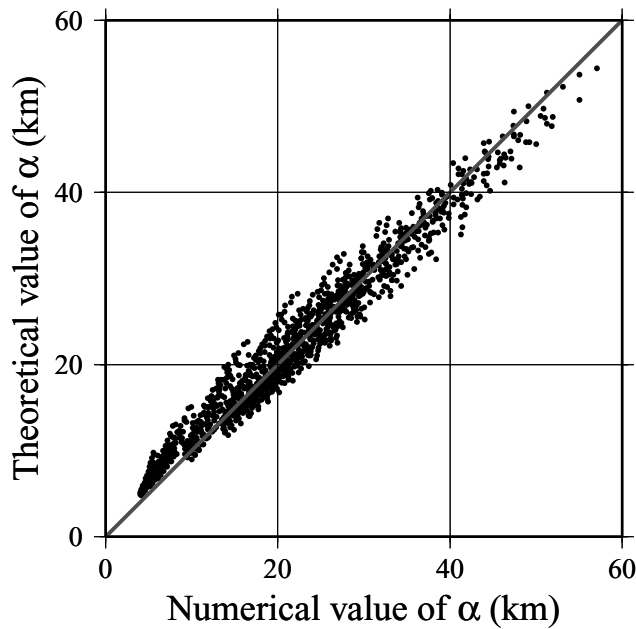
Figure 6. Comparison between the theoretical expression for the thickness, α (see eq. A21) of the advective boundary layer on top of the slab and the thickness determined from numerical solutions for the case in which free slip is allowed at the base of the overriding plate. The theoretical expression for the thickness of the advective boundary layer on top of the slab is given by the smaller of α (eq. A21) and $\pi\sqrt{\kappa t}$, where $t = r/V$ is the length of time for which the top of the slab has been in contact with the wedge. Numerical solutions are obtained for slab dips between $10°$ and $80°$, for convergence speeds between 10 and 100 mm yr^{-1}. In all cases the thickness, a, of the slab is taken to be 100 km, and the depth to the wedge corner, z_w, is 40, 60 or 80 km. Numerical values for boundary layer thickness were obtained by fitting profiles perpendicular to the top of the slab, starting where the top of the slab was at depths between z_w and 300 km. Solutions are not plotted in the cases where the descent speed was so slow ($V \sin\delta \lesssim 10$ mm yr^{-1}) that no error function could be fitted to the profile, or when heat flux from within the slab varies appreciably with distance along the slab ($t > a^2/\pi^2\kappa$).

z_w. This temperature gradient is consistent with the metamorphic conditions inferred from blueschists and eclogites believed to have been exhumed from subduction zones (e.g. Peacock 1992; Fryer *et al.* 1999), and with the inference, from the distribution of depths of thrust-faulting earthquakes, that temperatures of 400–600 °C are obtained at depths of 40–50 km on convergent plate boundaries (Tichelaar & Ruff 1993).

In Fig. 7 we compare the profiles of temperature along the top of the slab with and without this proxy for dissipative heating. We can see that, although the extra heating causes considerable increase in temperature along the plate boundary (depth, z, $\lesssim z_w$), the increases at greater depth are modest, being mostly 100 °C or less. This result shows, as would be expected from the arguments made at the beginning of this subsection, that dissipation can contribute significantly to heating near the plate boundary but once the slab has penetrated 100–200 km into the mantle the advection of heat by flow in the wedge is the dominant influence on the temperature structure.

Greater influence of dissipative heating on the thermal state of the top of the slab has been suggested in the past, particularly by Peacock *et al.* (1994), who postulated shear stresses on the top of the slab of 10–100 MPa down to depths of 150 km or more. Such distributions of stress yield total rates of dissipation of up to $6 \times$

10^5 W m^{-1}, far in excess of the estimates quoted above for the rates of dissipation on plate boundaries.

4 PETROLOGICAL IMPLICATIONS

We now return to the evidence for systematic variation in the depth of the slab beneath the fronts of volcanic arcs, which motivated this study. England *et al.* (2004) found that the top of the intermediate-depth seismicity beneath island arcs (which is close to the top of the slab (e.g. Engdahl & Gubbins 1987; Abers 1992; Zhao *et al.* 1994, 1997; Helffrich & Abers 1997; Igarishi *et al.* 2001)) lies at a depth that varies significantly from arc to arc and is strongly negatively correlated with $V \sin\delta$. The observations of England *et al.* (2004) are summarized in Table 2, with the exclusion of three arcs that exhibit significant back-arc spreading (see Section 3.4.1).

Our scaling arguments suggest that the places at which the tops of slabs reach a given temperature will all be at the same dimensionless distance $Vr\delta^2/\kappa$ from the wedge corner and that the maximum temperature in the mantle wedge, T_1, also depends upon $Vr\delta^2/\kappa$. The distance, r, from the wedge corner cannot be measured directly but can be calculated from the depth to the top of the slab, D, and the dip, δ, if the depth of the wedge corner, z_w, is assumed: $r = (D - z_w)/\sin\delta$. We take a value of 50 km for z_w, approximately the maximum depth of thrust-faulting at subduction zones (e.g. Tichelaar & Ruff 1993), and plot r, estimated for the top of the slab beneath the volcanic fronts, against $V\delta^2$ (Fig. 8). There is strong negative correlation between these two quantities and the data lie close to a line of slope -1, which is the relation expected if the location of arcs were controlled by maximum temperatures in the wedge that depended on $V\delta^2/r$ (as described by eqs 15 and 16).

Note that the correlation between $V\delta^2$ and r is very similar to the correlation between $V \sin\delta$ and D observed by England *et al.* (2004) because

$$\frac{Vr\delta^2}{\kappa} = \frac{V(D - z_w)\delta^2}{\kappa \sin\delta} \sim \frac{V(D - z_w)\sin\delta}{\kappa} \tag{20}$$

for $\sin\delta \sim \delta$.

The strong negative correlation between r and $V\delta^2$ (Fig. 8) implies that the locations of the arcs are controlled by a temperature-dependent process in the subduction zones that conforms to the scaling we have developed here. If this implication is correct, we may use our scaling relations to draw conclusions about the temperature regime beneath island arcs and, hence, about the petrological processes occurring there. We do not expect temperatures given by our scaling relations to agree precisely with their counterparts in the real world. Each temperature discussed below is uncertain by at least 100 °C, given the limitations of our approximation (Figs 3 and 4) and there is, doubtless, additional inaccuracy due to the simplicity of the model. However, more complex models exhibit variations in temperature of significantly more than 100 °C as parameters are varied (e.g. van Keken *et al.* 2002). Given the uncertainty in values of key parameters, such as those determining rheology, it is hard to tell which ranges of these more 'realistic' models lie closer to reality than our simple solutions.

4.1 Temperature on the top of the slab

A fundamental question about arc volcanism concerns the degree to which the material of the slab (sediment and/or hydrated oceanic crust) melts, and whether differences in subduction zone parameters, such as convergence speed, dip, and age of the slab can influence such melting. Estimates of the conditions required for oceanic
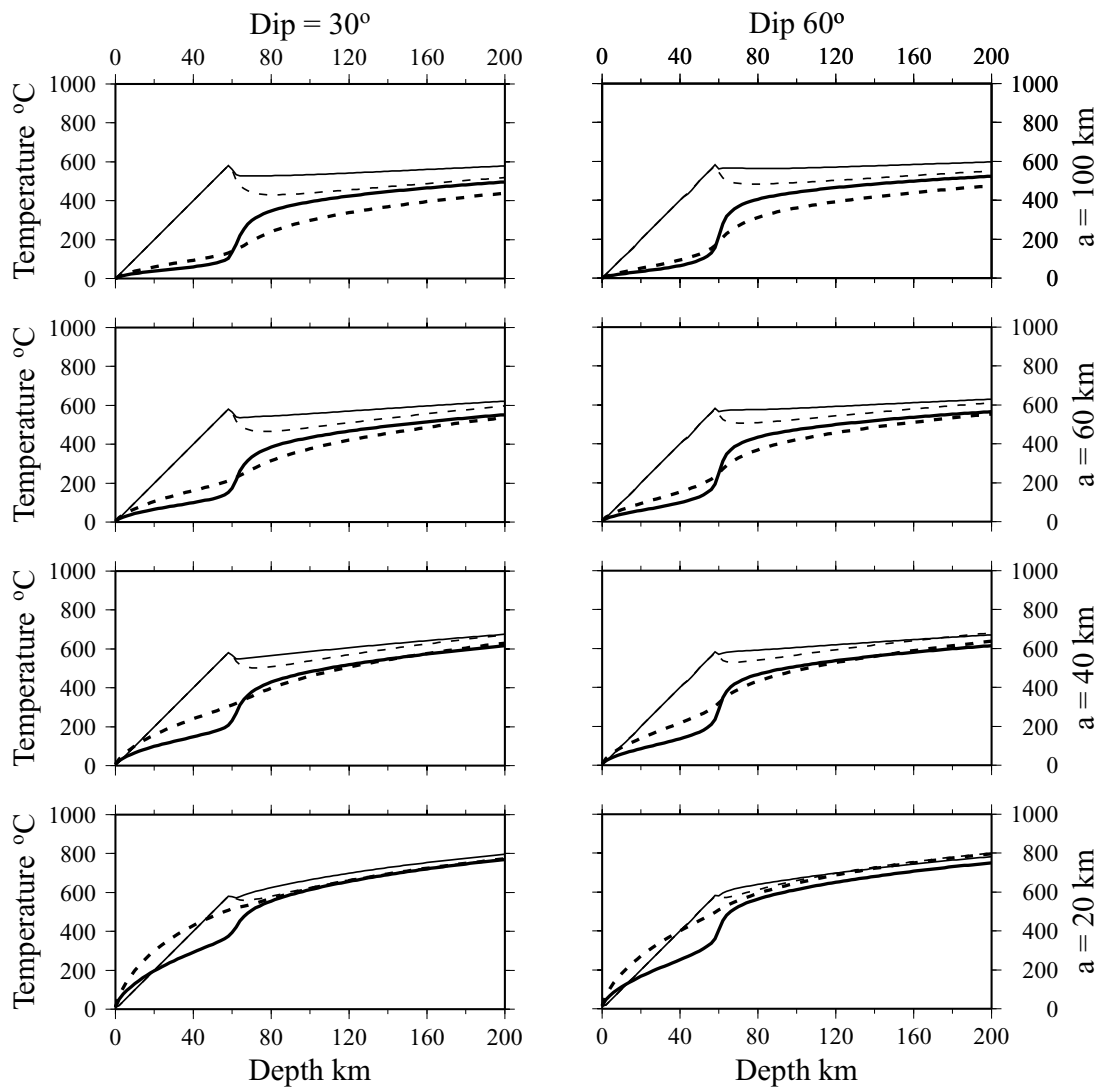
Figure 7. Profiles of temperature along the top of the slab for $\delta = 30°$, $60°$ and $a = 20, 40, 60$ *and* 100 km, with $z_w = 60$ km. In all panels, curves illustrate the temperature for $V = 30$ mm yr^{-1} (dashed) and 100 mm yr^{-1} (solid); thick curves show temperatures calculated as in Fig. 5 and thin curves show temperatures calculated with the plate boundary held at a temperature of 10 °C km^{-1} to a depth of 60 km.

sediment to melt have been made by Nichols *et al.* (1994), who suggest that the solidus lies at about 650 °C at a depth of 100 km, rising to about 720 °C at 200 km and, more recently by Johnson & Plank (1999), who conclude that temperatures approximately 100 °C higher than these may be appropriate. We use the solidus of Schmidt & Poli (1998) for H_2O-saturated basaltic crust; this lies at about 750 °C at 100 km, rising to about 900 °C at 200 km.

The scaling for temperature on the top of the slab is discussed in Section 3.3, in which we emphasize that the temperature within any subduction zone is expected to vary only slowly with depth, and that differences, between subduction zones, in the temperature at any depth will be slight unless the slab is young. These considerations are illustrated in Fig. 9 by plotting the temperature, at depths of 100, 150, 200 and 250 km, as a function of plate age and the quantity $V\delta^2$, using (17). Fig. 9 also shows the parameters for the subduction zones listed in Table 2.

According to the calculations illustrated here, the conditions at the tops of the slabs beneath these island arcs are too cold for the melting either of sediment or of H_2O-saturated oceanic crust. We recall,

however, that the temperatures derived from scaling arguments may be inaccurate by 100 °C or more. If all the calculated isotherms in Fig. 9 were raised by 100 °C, then the conditions determined by Nichols *et al.* (1994) for melting pelagic sediments would be met, for some of the subduction zones, when the top of the slab reaches depths between 200 and 250 km, though the conditions determined by Johnson & Plank (1999) would not be met.

The conditions for melting of H_2O-saturated oceanic crust are not satisfied at any depth illustrated in Fig. 9 for the arcs investigated by England *et al.* (2004). None of those arcs, however, contains slab of age younger than 40 Myr; subduction zones containing slabs younger than this age do not yield enough intermediate-depth earthquakes for the analysis employed by those authors. The large symbol A in Fig. 9 indicates the approximate position in parameter space occupied by the subduction zones of southwest Japan, southernmost Chile and the Cascades. These are all regions in which it is inferred that melting of oceanic crust contributes to the volcanism (e.g. Defant & Drummond 1990; Drummond & Defant 1990; Grove *et al.* 2001; Tatsumi *et al.* 2001).

Table 2. Parameters of volcanic arcs. Two-letter codes identify arc segments in Figs 9 and 10.

Code	Name	Depth, D^a	Dip, δ^b	V^c	Age^d
EA	E. Aleutians	65	61°	65	60
CA	C. Aleutians	80	61°	61	55
NK	N. Kuriles	80	49°	79	120
EP	E. Alaska Pen.	85	57°	56	46
AP	W. Alaska Pen.	95	50°	63	46
KA	Kamchatka	95	54°	76	90
GU	Guatemala	100	55°	67	25
JP	Japan	100	34°	88	124
SK	S. Kuriles	100	48°	71	120
SS	S. Sumatra	100	56°	61	80
JA	Java	100	40°	72	130
WA	W. Aleutians	105	61°	44	60
RY	Ryukyus	105	55°	49^e	47
CC	C. Chile	110	30°	67	34
NZ	New Zealand	110	50°	36	100
SP	S. Peru/N. Chile	115	35°	68	50
NS	N. Sumatra	115	37°	47	50
WI	West Indies	115	47°	19^f	70
BO	Bonin	120	42°	30^e	140
AE	Aegean	125	43°	43^g	120
IZ	Izu	130	47°	51^e	140

[a] Average depth to the top of intermediate earthquakes below volcanoes of island arcs, in kilometres (England *et al.* 2004).

[b] Average dip of the seismic zone between a depth of 80 km and 400 km or the termination of intermediate-depth seismicity, whichever is the shallower (England *et al.* 2004).

[c] Average rate of convergence, in millimetres per year, between the two plates bordering the arc, from the angular velocities of DeMets *et al.* (1994); the plate relative velocity is resolved perpendicular to the best-fitting small circle through the volcanic arc (England *et al.* 2004). Uncertainties represent the range in V along the arc segment. Rates for arcs bordering the Philippine Plate ([e]) are calculated from the angular velocities of Seno *et al.* (1993) for the Philippine Plate with respect to its surrounding plates. The rate for the Lesser Antilles ([f]) is calculated from the angular velocity of DeMets *et al.* (2000). The rate for the Aegean ([g]) is calculated from the Aegean–Eurasia angular velocity of Le Pichon *et al.* (1995) and the Africa–Eurasia angular velocity of DeMets *et al.* (1994).

[d] Average of the age of ocean floor entering the trench (Mueller *et al.* 1997).

For the reasons given in Section 3.3, if the slab is older than about 40 Myr variations in convergence rate and dip of the slab have very little influence on the temperature at the top of the slab. Fig. 9 shows, however, that the increase in temperature at the top of the slab that arises when the ocean floor is younger than 20 Myr can be as much as 300–400 °C: sufficient to cause melting of the basaltic crust. Thus the analysis we employ here supports the suggestions of previous workers that temperatures on the top of the slab become high enough to generate melting of the basaltic crust only where the ocean floor is younger that about 20 Myr (e.g. Defant & Drummond 1990; Drummond & Defant 1990; Peacock *et al.* 1994), or close to the ends of slab segments, where hot upper mantle can leak around the edges of the slab (Yogodzinski *et al.* 2001). It is also highly probable that the influence of temperature-dependent rheologies will be to raise temperatures at the top of the slab to higher values than we obtain with a constant-viscosity fluid (e.g. van Keken *et al.* 2002).

An additional implication of Fig. 9 is that melting of material of the slab is not the trigger for arc volcanism. The depth of the slab beneath island arcs varies significantly from arc to arc, and is strongly negatively correlated with its speed of descent (Fig. 8 and eq. 20). Regardless of the uncertainties in the absolute value
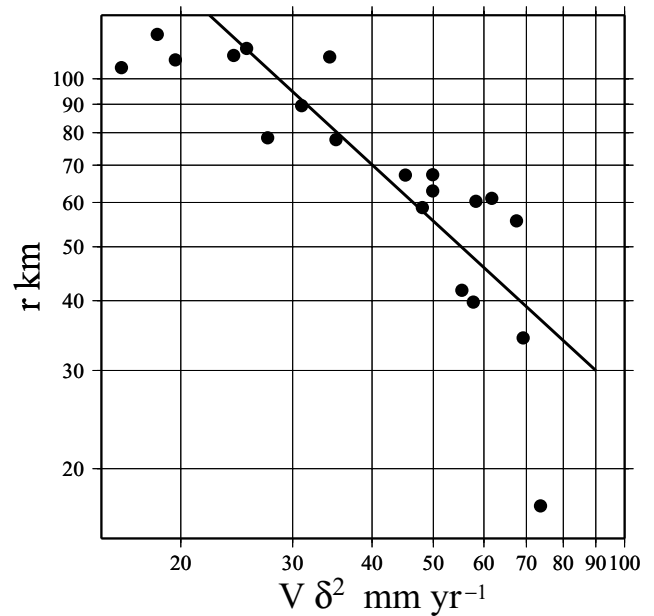
Figure 8. The parameters of volcanic fronts above subduction zones studied by England *et al.* (2004). The radial distance between the top of the slab beneath each individual arc segment and the wedge corner ($r = (D - z_w)/\sin\delta$, where z_w is taken to be 50 km) is plotted against $V\delta^2$ (see Table 2). The solid line has a slope of -1 on the log–log plot.

of temperature derived from scaling arguments, our analysis shows that the temperature on the top of the slab at any depth depends very weakly on convergence rate and slab dip (Section 3.2), and thus that the observed correlation could not be generated in any simple way by the onset of melting of slab material, nor by any other strongly temperature-dependent process taking place on the top of the slab. It is probable that melting of sediment does contribute to arc magmatism (see, for example, Johnson & Plank 1999), but Fig. 9 suggests that this melting may be initiated when the slab has passed beyond the volcanic front (perhaps to depths of 150 km or more) and that melt travels back towards the volcanic front through the wedge. This suggestion is consistent with the inferences, from body-wave tomography beneath Japan, of inclined channels of low wave speed leading from the slab at depths around 150 km to beneath the arc volcanoes (e.g. Hasegawa *et al.* 1991; Iwamori & Zhao 2000; Wyss *et al.* 2001).

4.2 Temperatures in the wedge

Fig. 10 shows the variation of maximum temperature in the wedge (given by eq. 15) as a function of distance from the wedge corner, r, and the quantity $V\delta^2$. The figure also plots the values of these parameters for the top of the slab beneath the volcanic front in the subduction zones listed in Table 2. It is evident from this figure that if our scaling is relevant to active subduction zones then the fronts to the volcanic arcs investigated lie above portions of the wedge whose maximum temperatures are within a narrow range of about 150 °C. Although the figure suggests that this range is about 950–1100 °C, we must recall that the absolute values of the temperatures we estimate are uncertain by at least 100 °C. Let us, for example, assume that the algebraic form of the scaling is correct but that the values of constants in the relations may vary. If, instead of using a value of 400 for the numerical constant in (15), we were to use a value of 300, then the relevant temperature range becomes
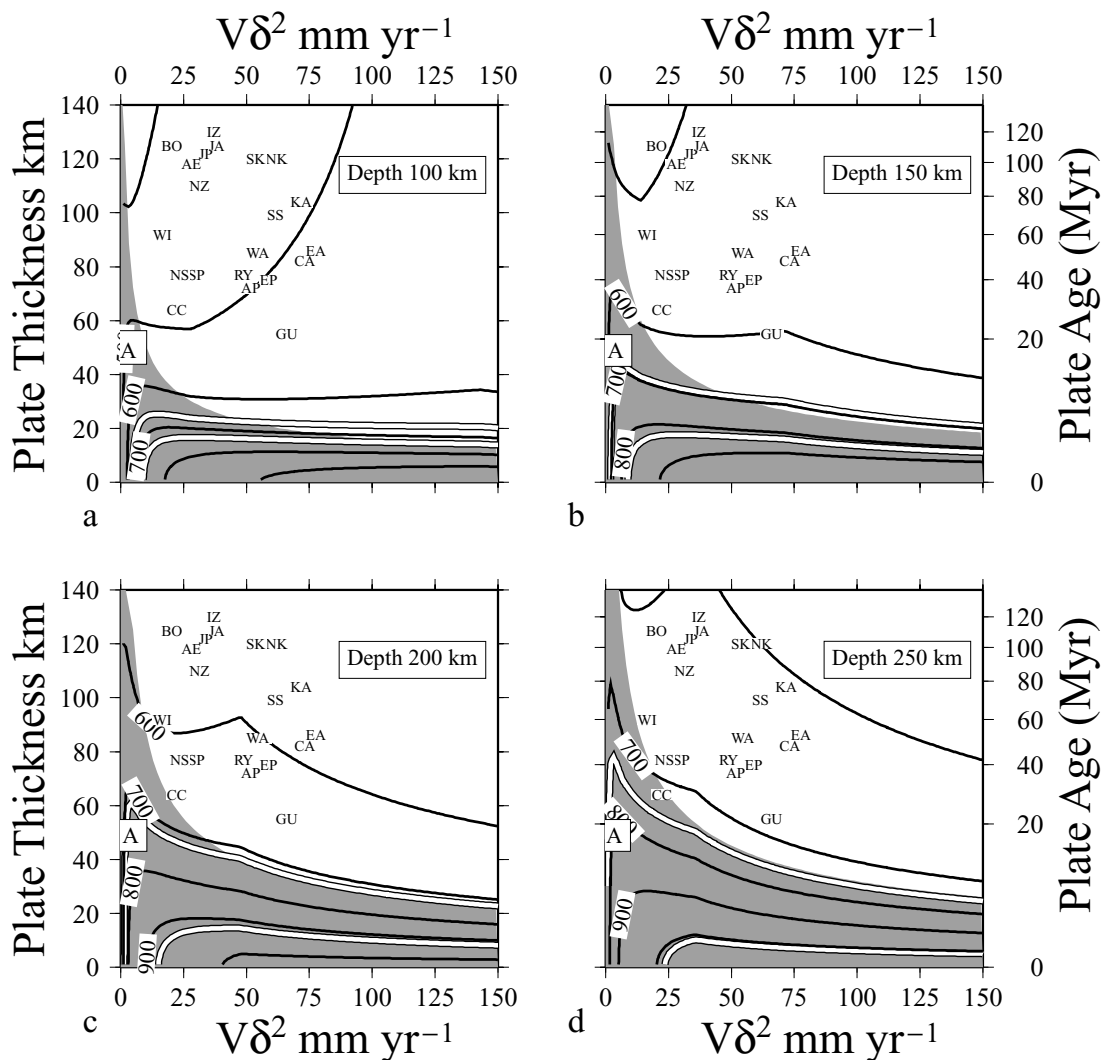
Figure 9. Theoretical values of temperature on the top of the slab, calculated using (17), with T_1 given by (15), as a function of convergence rate, V, and plate thickness, a; z_w is fixed at 50 km and δ is fixed at $\pi/4$. Depth to the top of the slab is 100 km (a), 150 km (b), 200 km (c) and 250 km (d). To enable comparison with the experimental solidi, an adiabatic gradient of 0.6 °C km^{-1} is added to the temperatures. Slab thickness, a, is converted to effective age of the oceanic lithosphere by the relation $a \sim 11$ km $\times \sqrt{\text{age (Myr)}}$ or $a = 125$ km, whichever is the smaller. The shaded regions correspond to parts of parameter space in which the maximum depth of penetration of the slab would be comparable to the depth considered, thus the calculated temperatures would probably underestimate the true temperatures of material at the top of the slab (see text). The large letter A indicates the conditions of slab age and $V\delta^2$ that pertain to the Austral Andean zone, the Cascades and southwest Japan, taken from Jarrard (1986). Double curves indicate the approximate temperature contours corresponding to the solidi of pelagic sediment (lower temperatures (Nichols *et al.* 1994)) and H$_2$O-saturated basalt (higher temperatures (Schmidt & Poli 1998)). Segments are identified by a two-letter code: AEgean; AP, western Alaskan Peninsula; BOnin; Central Aleutians; Central Chile; East Aleutians; EP, Eastern Alaskan Peninsula; GUatemala; JaPan; JAva; KAmchatka; IZu; New Zealand; North Kuriles; North Sumatra; RYukyu; South Kuriles; South Peru; South Sumatra; West Aleutians; West Indies. Symbols EA, IZ, NS and AP are slightly misplaced from their correct positions for clarity.

1050–1200 °C; a value of 500 for the constant brings this range down to 900–1050 °C.

The fact that, in $V\delta^2 - r$ space, the positions of the top of the slab beneath present island arcs lie close to the positions of a narrow range of isotherms of peak temperatures in the wedge suggests that the location of the volcanic front is controlled by a temperature-dependent process in the wedge. Mechanisms have been proposed that seem at least qualitatively consistent with this conclusion. Several authors have suggested that the release of fluid in strongly temperature-dependent reactions may explain the locus of arc volcanism; candidate reactions include the dehydration of serpentine or lawsonite and the liberation of fluid by the partial melting of sedimentary material or hydrated oceanic crust within the slab (e.g. Nichols *et al.*

1994; Ulmer & Trommsdorff 1995; Iwamori 1998; Johnson & Plank 1999; Kerrick & Connolly 2001). Most of these candidate reactions would, however, take place in the top of the slab or in the advective boundary layer on top of the slab. As we discuss above, the gradual increase of temperature along the top of the slab means that a temperature-dependent process taking place there is an unpromising mechanism for producing sharp localization of the volcanic front. In contrast, each isotherm within the wedge is sharply convex towards the wedge corner (Fig. 1), thus if a strongly temperature-dependent process in the wedge controls the generation or ascent of magma beneath the arcs then the closest approach of this critical temperature to the trench will be at the localized 'nose' of the relevant isotherm. For example, Schmidt & Poli (1998), emphasizing the large number
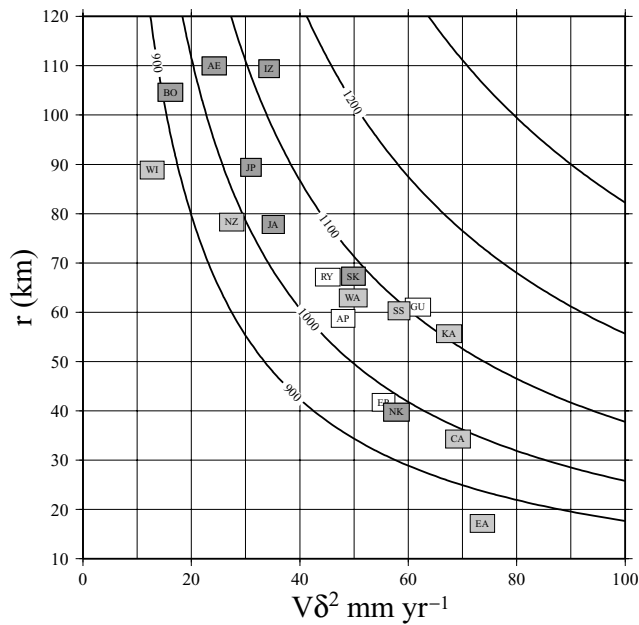
Figure 10. Contours of maximum value of temperature in the wedge calculated from (15), with the slab being 100 km thick; an adiabatic gradient of $0.6\,^{\circ}\mathrm{C}\,\mathrm{km}^{-1}$ is added to the temperatures. Squares indicate the approximate values of $V\delta^2$ and r for subduction zones listed in Table 2. White squares correspond to arcs in which ocean floor at the trench is younger than 50 Myr; for light grey squares the age lies between 50 and 100 Myr; for dark grey squares, the age is greater than 100 Myr. Refer to the caption to Fig. 9 or to Table 2 for two-letter abbreviations for arcs.

of potential dehydration reactions in slab and upper mantle, postulate localization of the volcanic front above an isotherm in the wedge where the extent of melting is great enough to allow extraction of the melt.

5 CONCLUSIONS

There have been many investigations of the thermal state of subduction zones but, almost without exception since the pioneering studies of McKenzie (1969) and Turcotte & Schubert (1973), they have relied on numerical solutions to the equations. Numerical solutions have the superficial attraction of being able to handle complex details of geometry, of rheology, of heat transport and of petrological processes. Such complex models, however, have the often-neglected disadvantage that, without an underpinning analytical framework, they are impossible to understand. Analytical solutions, while necessarily idealized, offer insights into the processes through the transparent relation between governing parameters and the solutions to the equations, and through the relative ease with which their parameter space may be explored. The analytical approximations to temperatures that we have developed here allow us to make general statements about the temperatures in subduction zones, and to draw inferences about the processes governing the location of the volcanic arcs.

In our simplified model, the temperature of the top of the slab, T_s, the maximum temperature on a profile through the wedge perpendicular to the slab, T_1, and the thickness of the advective boundary layer on top of the slab, α, all depend on the dimensionless distance from the wedge corner, $Vr\delta^2/\kappa$, where V is the convergence rate, r is radial distance from the wedge corner, δ is the dip of the slab and

κ is thermal diffusivity (Fig. 1 and Table 1). Numerical experiments show that these analytical approximations adequately describe the variation of temperatures with the parameters of subduction over the full range relevant to active subduction zones (Figs 2 to 4).

The observation that the radial distance, r, between the top of the intermediate-depth seismicity beneath the volcanic fronts and the wedge corner at active subduction zones is strongly negatively correlated with $V\delta^2/\kappa$ (Fig. 8 and its discussion) suggests that the location of the arcs is controlled by a strongly temperature-dependent process taking place either at the top of the slab or in the wedge of mantle beneath the arcs. Our analytical solutions allow us to distinguish between these possibilities. The temperature at the top of the slab depends only weakly upon the convergence rate, V, and dip, δ, of the slab (Fig. 9 and its discussion), thus one would not expect any temperature-dependent process occurring at the top of the slab to exhibit the sharp localization that characterizes the positions of the volcanic arcs. In contrast, each isotherm in the wedge is strongly convex towards the wedge corner (Fig. 1) and thus the closest approach to the trench of any isotherm in the wedge is strongly localized. Because the maximum temperature in the mantle wedge depends strongly on $Vr\delta^2/\kappa$ (15), we conclude that the negative correlation between $V\delta^2/\kappa$ and r shown in Fig. 8 implies that a temperature-dependent process in the mantle wedge is responsible for the focusing of volcanic activity at the sharp fronts to the arcs (Fig. 10). We do not speculate about what that process might be, but suggest that the observations of England *et al.* (2004), combined with the scaling arguments of this paper, may provide strong constraints for petrological modelling of the generation of island-arc magmas.

REFERENCES

Abers, G.A., 1992. Relationship between shallow- and intermediate-depth seismicity in the eastern Aleutian subduction zone., *Geophys. Res. Lett.,* **19,** 2019–2022.

Batchelor, G.K., 1967. *An Introduction to Fluid Dynamics,* Cambridge University Press, Cambridge.

Carslaw, H.S. & Jaeger, J.C., 1959. *Conduction of Heat in Solids,* 2nd edn, Oxford University Press, Oxford.

Davies, H. & Stevenson, D., 1992. Physical model of the source region of subduction volcanics, *J. geophys. Res.*, **97,** 2037–2020.

Davies, J.H., 1999. Simple analytical model for subduction zone thermal structure, *Geophys. J. Int.,* **139,** 823–828.

Defant, M.J. & Drummond, M.S., 1990. Derivation of some modern arc magmas by melting of young subducted lithosphere, *Nature,* **347,** 662–665.

DeMets, C., Gordon, R., Argus, D. & Stein, S., 1994. The effect of recent revisions to the geomagnetic reversal time scale on estimates of current plate motions, *Geophys. Res. Lett.,* **21,** 2191–2194.

DeMets, C., Jansma, P., Mattioli, G., Dixon, T., Farina, F., Bilham, R., Calais, E. & Mann, P., 2000. GPS geodetic constraints on Caribbean–North America plate motion, *Geophys. Res. Let.,* **21,** 2191–2194.

Drummond, M.S. & Defant, M.J., 1990. A model for trondhjemite–tonalite–dacite genesis and crustal growth via slab melting: Archaean to modern comparisons, *J. geophys. Res.,* **95,** 21 503–21 521.

Engdahl, E. & Gubbins, D., 1987. Simultaneous travel time inversion for earthquake location and subduction zone structure in the central Aleutian islands, *J. geophys. Res.,* **92,** 13 855–13 862.

England, P. & Molnar, P., 1991. Inferences of deviatoric stress in actively deforming belts from simple physical models, *Phil. Trans. R. Soc. Lond.,* **337,** 151–164.

England, P.C., Engdahl, E.R. & Thatcher, W., 2004. Systematic variation in the depths of slabs beneath arc volcanoes, *Geophys. J. Int.,* **156,** 377–408.

Fryer, P., Wheat, C.G. & Mott, M.J., 1999. Mariana blueschist mud volcanism: implications for conditions within the subduction zone, *Geology, 27,* 103–106.

Furukawa, Y., 1993. Magmatic processes under arcs and formation of the volcanic front, *J. geophys. Res.,* **98,** 8309–8319.

Grove, T.L., Parman, S.W., Bowring, S.A., Price, R.C. & Baker, M.B., 2001. The role of an H_2O-rich fluid component in the generation of primitive basaltic andesites and andesites from the Mt. Shasta region, N California, *Contrib. Mineral. Petrol.*

Hasegawa, A., Zhao, D., Hori, S., Yamamoto, A. & Horiuchi, S., 1991. Deep structure of the northeastern Japan arc and its relation ship to seismic and volcanic activity, *Nature,* **352,** 683–690.

Helffrich, G. & Abers, G.A., 1997. Slab low-velocity layer in the eastern Aleutian subduction zone, *Geophys. J. Int.,* **130,** 640–648.

Igarishi, T., Matsuzawa, T., Umino, N. & Hasegawa, A., 2001. Spatial distribution of focal mechanisms for interplate and intraplate earthquakes associated with the subducting Pacific plate beneath the northeastern Japan arc: a triple-planed deep seismic zone, *J. geophys. Res.,* **106,** 2177–2191.

Iwamori, H., 1998. Transportation of H_2O and melting in subduction zones, *Earth planet. Sci. Lett.,* **160,** 65–80.

Iwamori, H. & Zhao, D., 2000. Melting and seismic structure beneath the northeast Japan arc, *Geophys. Res. Let.,* **27,** 425–428.

Jarrard, R.D., 1986. Relations among subduction parameters, *Rev. Geophys.,* **24,** 217–284.

Jarvis, G. & McKenzie, D.P., 1980. Convection in a compressible fluid with an infinite Prandtl number, *J. Fluid Mech.,* **96,** 515–583.

Johnson, C., 1990. *Numerical Solution of Partial Differential Equations by the Finite Element Method,* Cambridge University Press, Cambridge.

Johnson, M.C. & Plank, T., 1999. Dehydration and melting experiments constrain the fate of subducted sediments, *Geochem. Geophys. Geosyst.,* **1,** doi:10.1029/1999/GC000014.

Kerrick, D. & Connolly, J., 2001. Metamorphic devolatilization of subducted oceanic metabasalts: implications for seismicity, arc magmatism, and volatile recycling, *Earth planet. Sci. Lett.,* **189,** 19–29.

Le Pichon, X., Chamot-Rooke, N., Lallemant, S., Noomen, R. & Veis, G., 1995. Geodetic determination of the kinematics of central Greece with respect to Europe: Implications for Eastern Mediterranean tectonics, *J. geophys. Res.,* **100,** 12 675–12 690.

McKenzie, D., 1969. Speculations on the consequences and causes of plate motion, *Geophys. J. R. astr. Soc.,* **18,** 1–32.

McKenzie, D. & Jarvis, G., 1980. The conversion of heat into mechanical work by convection, *J. geophys. Res.,* **85,** 6093–6096.

Mitrovica, J. & Forte, A., 1997. Radial profiles of mantle viscosity: results from joint inversion of convection and postglacial rebound observations, *J. geophys. Res.,* **102,** 2751–2769.

Molnar, P. & England, P., 1990. Temperatures, heat flux, and frictional stress near major thrust faults, *J. geophys. Res.,* **95,** 4833–4856.

Mueller, R.D., Roest, W.R., Royer, J.-Y., Gahagan, L.M. & Scalter, J.G., 1997. Digital isochrons of the world oceans, *J. geophys. Res.,* **102,** 3211–3214.

Nichols, G., Wyllie, P. & Stern, C., 1994. Subduction zone melting of pelagic sediments constrained by melting experiments, *Nature,* **371,** 785–788.

Peacock, S.M., 1992. Blueschist-facies metamorphism, shear heating, and *P–T–t* paths in subduction shear zones, *J. geophys. Res.,* **97,** 17 693–17 707.

Peacock, S.M., Rushmer, T. & Thompson, A.B., 1994. Partial melting of subducting oceanic crust, *Earth planet. Sci. Lett.,* **121,** 227–244.

Ribe, N., 1989. Mantle flow induced by back arc spreading, *Geophys. J. Int.,* **98,** 85–91.

Schmidt, M.W. & Poli, S., 1998. Experimentally based water budgets for dehydrating slabs and consequences for arc magma generation, *Earth planet. Sci. Lett.,* **163,** 361–379.

Seno, T., Stein, S. & Gripp, A., 1993. A model for the motion of the Philippine plate consistent with NUVEL1 and geological data, *J. geophys. Res.,* **98,** 17 941–17 948.

Tatsumi, Y., Ishikawa, N., Anno, K., Ishizaka, K. & Itaya, T., 2001. Tectonic setting of high-Mg andesite magmatism in the SW Japan arc: K–Ar chronology of the Setouchi volcanic belt, *Geophys. J. Int.,* **144,** 625–631.

Tichelaar, B.W. & Ruff, L., 1993. Depth of seismic coupling along subduction zones, *J. geophys. Res.,* **98**(B9), 2107–2037.

Tovish, A., Schubert, G. & Luyendyk, B., 1978. Mantle flow pressure and the angle of subduction: non-Newtonian corner flows, *J. geophys. Res.,* **83,** 5892–5898.

Turcotte, D.L. & Schubert, G., 1973. Frictional heating of descending lithosphere, *J. geophys. Res.,* **78,** 5876–5886.

Ulmer, P. & Trommsdorff, V., 1995. Serpentine stability to mantle depths and subduction-related magmatism, *Science,* **268,** 858–861.

van Keken, P.E., Kiefer, B. & Peacock, S.M., 2002. High resolution models of subduction zones: implications for mineral dehydration reactions and transport of water into the deep mantle, *Geochem. Geophys. Geosyst.,* **210,** 1056, doi:/2001/GC000256.

Von Herzen, R., Ruppel, C., Molnar, P, Nettles, M., Nagihara, S. & Ekström, G., 2001. A constraint on the shear stress at the Pacific–Australian plate boundary from heat flow and seismicity at the Kermadec forearc, *J. geophys. Res.,* **106,** 6817–6833.

Wessel, P. & Smith, W.H.F., 1998. New, improved version of generic mapping tools released, *EOS, Trans. Am. geophys. Un.,* **79,** 579.

Wyss, M., Hasegawa, A. & Nakajima, J., 2001. Source and path of magma for volcanoes in the subduction zone of northeastern Japan, *Geophys. Res. Lett.,* **28,** 1819–1822.

Yogodzinski, G.M., Lees, J.M., Churikova, T.G., Dorendorf, F., Woerner, G. & Volynets, O.N., 2001. Geochemical evidence for the melting of subducting oceanic lithosphere at plate edges, *Nature,* **409,** 500–504.

Zhao, D., Hasegawa, A. & Kanamori, H., 1994. Deep structure of Japan subduction zone as derived from local, regional, and teleseismic events, *J. geophys. Res.,* **99,** 22 313–22 330.

Zhao, D., Matsuzawa, T. & Hasegawa, A., 1997. Morphology of the subducting slab boundary in the northeastern Japan arc, *Phys. Earth planet. Inter.,* **102,** 89–104.

APPENDIX A: ANALYTICAL EXPRESSIONS FOR TEMPERATURES AT THE TOP OF THE SLAB AND IN THE WEDGE

In this appendix we derive approximate expressions for the temperature along the top of the slab, and in the wedge of mantle above the slab. As a preliminary to our analysis we obtain approximate expressions for the component of velocity in the wedge that is perpendicular to the slab. We use the balance between diffusion and advection of heat perpendicular to the top of the slab to derive an expression for the temperature in the advective boundary layer on top of the slab. We find that the temperature at the top of the slab scales with the maximum temperature in the interior of the wedge above the slab. We then use the balance between radial advection of heat in the wedge and diffusion of heat out of the wedge through the bounding plates to show that the maximum temperature in the wedge scales with dimensionless distance $V r \delta^2 / \kappa$, where V is convergence rate, δ is dip of the slab, κ is thermal diffusivity and r is distance from the wedge corner.

A1 Expressions for velocity in the wedge

The approximate solutions we obtain for temperature in the slab and wedge are governed by the advection of heat towards the slab by flow in the wedge. We therefore need to know the component of velocity, u_x, perpendicular to the slab:

$$u_x = u_r \sin(\theta - \delta) - u_\theta \cos(\theta - \delta), \tag{A1}$$

where radial and tangential components of the velocity in the wedge (u_r, u_θ) are expressed in terms of derivatives of the stream function (2)–(5), and x is measured perpendicular to the top of the slab, in the upward $(-\theta)$ direction.

For transparency of our solutions, we seek a simplification of this expression. We cast our expression in terms of the angular distance, $\phi = \delta - \theta$, measured from the top of the slab. Substituting for u_r and u_θ, and rearranging, we obtain

$$u_x = V \frac{\sin^2 \phi \left(\frac{1}{2} \sin 2\delta - \delta \right) + \sin^2 \delta \left(\phi - \frac{1}{2} \sin 2\phi \right)}{\delta^2 - \sin^2 \delta}. \tag{A2}$$

The form of u_x is shown in Fig. A1(a). We have been unable to simplify this expression usefully by any of the common expansions, but we note that the minimum (most negative) value of u_x is attained at $\phi \sim 2\delta/3$ (Fig. A1b), and we have determined empirically that this value is given by
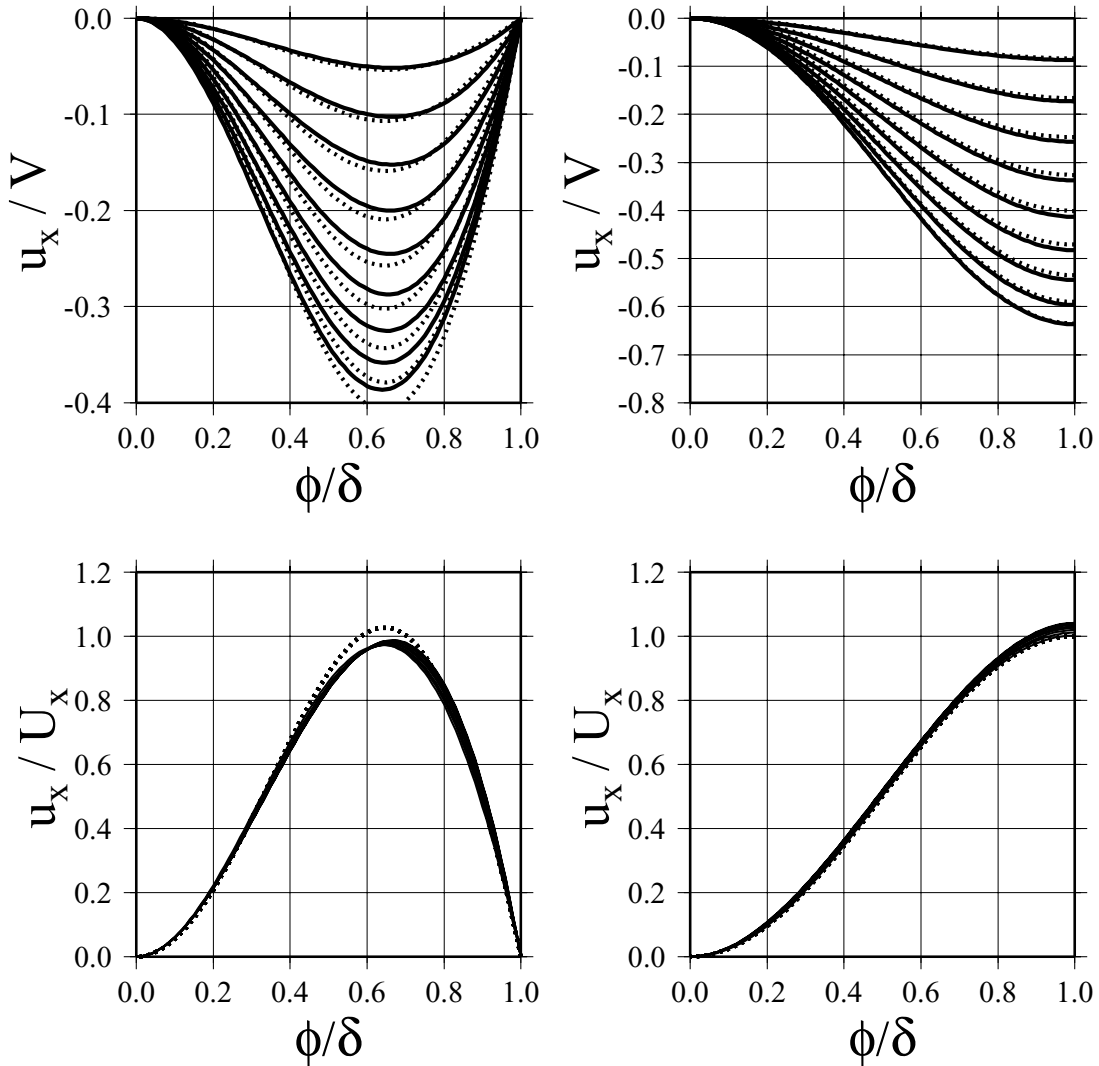
$$U_x \sim \frac{-V\delta\xi}{2}, \tag{A3}$$

where

$$\xi = 1 - \frac{2}{5} \sec(2\delta/5). \tag{A4}$$

For $0 < \delta < \pi/3$, $0.6 > \xi > 0.56$ and for $\pi/3 < \delta < \pi/2$, $0.56 > \xi > 0.51$. Furthermore, u_x may be approximated by

$$u_x \sim \frac{U_x}{2} \left[1 - \cos\left(\frac{3\pi\phi}{2\delta} \right) \right]. \tag{A5}$$

Fig. A1 shows that this approximation agrees with the full solution to within a few per cent as long as $\phi/\delta \lesssim 0.8$. We shall obtain a

Figure A1. (a) Solid curves show the component of velocity perpendicular to the slab, u_x/V, plotted against ϕ/δ given by eq. (A2). Dotted curves show the approximation given by eq, (A5). The nine pairs of curves correspond to $\delta = 10°$ (lowest) to $90°$ (highest), in steps of $10°$. (b) Solid and dotted curves show the full (eq. A1) and approximate (eq. A5) solutions divided by U_x (eq. A3). Again, solutions are shown for $\delta = 10°$ to $90°$, in steps of $10°$, though the curves overlap and obscure one another. Panels (c) and (d) as panels (a) and (b), but for free-slip condition on the base of the overriding plate (eq. A20).

solution below for the temperature as a function of distance, x, from the top of the slab; if a point on the top of the slab is a distance, r, from the wedge corner (Fig. 1),

$$u_x \sim \frac{U_x}{2}\left[1 - \cos\left(\frac{3\pi \arctan(x/r)}{2\delta}\right)\right], \tag{A6}$$

which may be approximated, for $x \lesssim r$, by

$$u_x \sim \frac{U_x}{2}\left[1 - \cos\left(\frac{3\pi x}{2r\delta}\right)\right]. \tag{A7}$$

A2 Thickness of the advective boundary layer

We assume that subduction has continued for long enough that the temperature at the top of the slab is in steady state. Because the gradients of temperature near the top of the slab are very small in the direction parallel to the slab, and steep in the direction perpendicular to the slab (Fig. 1) we make the approximation that advection and diffusion of heat perpendicular to the slab dominate over thermal diffusion parallel to the slab. In a frame of reference fixed to the top of the slab, the temperature equation becomes

$$\frac{d^2 T}{dx^2} - \frac{u_x}{\kappa}\frac{dT}{dx} = 0, \tag{A8}$$

where x is distance measured upward from, and perpendicular to, the top surface of the slab and κ is thermal diffusivity. Substituting for u_x from (A3), (A4), (A7) and (A8) become

$$\frac{d^2 T}{dx^2} + \frac{V\delta\xi}{4\kappa}\left[1 - \cos\left(\frac{3\pi x}{2r\delta}\right)\right]\frac{dT}{dx} = 0. \tag{A9}$$

The solution to (A9) is:

$$T(x) = A + B\int \exp\left\{\frac{V\delta^2\xi r}{6\pi\kappa}\left[\sin\left(\frac{3\pi x}{2r\delta}\right) - \frac{3\pi x}{2r\delta}\right]\right\}dx. \tag{A10}$$

Taking the first two terms of the sine expansion gives

$$T(x) \sim A + B\int \exp\left(\frac{-3\pi^2 V\xi x^3}{32\kappa r^2\delta}\right)dx, \tag{A11}$$

which suggests a solution of the form

$$T(x) \sim A + Bf\left(\frac{x}{x_0}\right), \tag{A12}$$

where

$$x_0 = \left(\frac{\kappa r^2\delta}{V\xi}\right)^{1/3}. \tag{A13}$$

Numerical evaluation shows that, for $\lambda \gtrsim 1$,

$$\int_0^x \exp\left\{\lambda\left[\sin\left(\frac{x'}{b}\right) - \frac{x'}{b}\right]\right\}dx' \sim I_\infty \mathrm{erf}\left(\frac{\lambda^{1/3}x}{\sqrt{\pi}b}\right), \tag{A14}$$

where

$$I_\infty = \int_0^\infty \exp\left\{\lambda\left[\sin\left(\frac{x'}{b}\right) - \frac{x'}{b}\right]\right\}dx'. \tag{A15}$$

In (A10), $\lambda = V\delta^2\xi\, r/6\pi\kappa$ and $b = 2r\delta/3\pi$. For subduction speeds of 10(100) mm yr^{-1} or greater, $\lambda \gg 1$ provided that r is greater than 3(0.3) km, so we may use (A14) to approximate (A10). Substituting for λ and b, we obtain

$$T(x) \sim A + B\, \mathrm{erf}\left(\frac{x}{\alpha}\right), \tag{A16}$$

where

$$\alpha = \left(\frac{16\kappa r^2\delta}{9\sqrt{\pi}V\xi}\right)^{1/3}. \tag{A17}$$

Let the temperature on the top of the slab ($x = 0$) be T_s and let the temperature in the interior of the wedge, at a great distance from the slab, be T_1 then:

$$T(x) = T_s + (T_1 - T_s)\,\mathrm{erf}\left(\frac{x}{\alpha}\right). \tag{A18}$$

The quality of this approximation is assessed in Section 3.1.

A.2.1 Boundary layer thickness for different assumptions about velocity in the wedge

When free slip is allowed at the base of the overriding plate (see eq. 5), the equivalent expression to (A3) for the maximum velocity perpendicular to the slab is

$$U_x \sim \frac{-4V\delta\xi}{5}, \tag{A19}$$

and its variation with distance from the top of the slab is given by

$$u_x \sim \frac{U_x}{2}\left[1 - \cos\left(\frac{\pi x}{\delta r}\right)\right]. \tag{A20}$$

Again, Fig. A1 shows that this approximation agrees with the full solution. The corresponding expression for the thickness, α, of the boundary layer is

$$\alpha = \left(\frac{5\kappa r^2\delta}{2\sqrt{\pi}V\xi}\right)^{1/3}. \tag{A21}$$

The expressions so far determined for α owe their details to a specific form, in (A7) and (A20), of the component of velocity perpendicular to the top of the slab. We should expect that, in the real situation of a subduction zone, the details of the flow would not follow exactly the corner flow investigated here, and it is worth investigating a more general form for u_x. We may imagine that any circulation driven by the descending slab will have a maximum in its component perpendicular to the top of the slab that scales with the speed, V, of the slab and perhaps, as in the case investigated here, with its dip, δ. Thus we may write, generally, that

$$U_x \sim -\epsilon V\delta^n,$$

where n may be zero, or a small number, and ϵ is a constant whose magnitude is perhaps between $1/\pi$ and 1. We may further reasonably imagine that u_x reaches its maximum value at an angle within the wedge that is approximately a constant fraction of δ and, as here, that the velocity near the boundary varies approximately as a power of distance from the boundary. Thus a simple general form for u_x might be

$$u_x \sim -\epsilon V\delta^n\left(\frac{\phi}{\delta}\right)^m \sim -\epsilon V\delta^n\left(\frac{x}{r\delta}\right)^m. \tag{A22}$$

As we describe in Section 3.1, an expression for the thickness of the thermal boundary layer is given by the requirement that the timescales for diffusion and advection across it are approximately equal. For a boundary layer of thickness α, these times are approximately equal to $\alpha^2/(\pi^2\kappa)$ and α/U, respectively, where U is the characteristic speed of the flow in the boundary layer. Substituting $U \sim u_x(\alpha)$ into the second of these timescales gives

$$\frac{\epsilon V\delta^{n-m}(\alpha/r^m)}{\alpha}\quad \frac{\alpha^2}{\pi^2\kappa} \sim 1, \tag{A23}$$

or

$$\alpha \sim r\delta \left(\frac{\pi^2 \kappa}{\epsilon V r \delta^{(n+1)}} \right)^{1/(m+1)}. \tag{A24}$$

A3 Temperature at the top of the slab

Following Davies & Stevenson (1992), we solve for T_s in (A18) by matching heat fluxes across the boundary $x = 0$. Differentiating (A18) with respect to x and multiplying by conductivity, K, gives the heat flux at the base of the advective boundary layer on top of the slab:

$$Q|_+ \sim \frac{2K}{\sqrt{\pi}} \left(\frac{T_1 - T_s}{\alpha} \right). \tag{A25}$$

We assume (see Section 2.2) that the temperature in the slab as it enters the subduction zone is

$$T(x) = -\frac{T_a x}{a} \qquad -a \le x < 0, \tag{A26}$$

$$T(x) = T_a \qquad x < -a. \tag{A27}$$

(Note the change in variable from eqs (6) and (7), in which z refers to depth beneath the Earth's surface; here x refers to distance above the top of the slab.) If the temperature at the top of the slab remained at zero, then this temperature profile would relax with time to give

$$
\begin{aligned}
T(x < 0, t) = T_a \Bigg\{ &\sqrt{\frac{\kappa t}{\pi a^2}} \left[\exp\left(-\frac{(x-a)^2}{4\kappa t} \right) \right. \\
&\left. - \exp\left(-\frac{(x+a)^2}{4\kappa t} \right) \right] \\
&- \frac{1}{2} \left[\left(1 - \frac{x}{a} \right) \mathrm{erf}\left(\frac{x-a}{2\sqrt{\kappa t}} \right) \right. \\
&\left. + \left(1 + \frac{x}{a} \right) \mathrm{erf}\left(\frac{x+a}{2\sqrt{\kappa t}} \right) \right] \Bigg\}
\end{aligned}
\tag{A28}
$$

$$\left. \frac{\partial T}{\partial x} \right|_{x=0} = -\frac{T_a}{a} \mathrm{erf}\left(\frac{a}{2\sqrt{\kappa t}} \right). \tag{A29}$$

However, the top of the slab is heated through contact with the overriding plate, and by heat advected towards it by the wedge. Profiles of the temperature along the top of the slab (Fig. 5) show two types of behaviour. For high descent speeds, and when the slab is thick, the top of the slab warms only very slowly as it is thrust beneath the overriding plate, but then warms rapidly as it comes into contact with the wedge, so the profile shows a sharp kink at the depth of the base of the overriding plate. At lower descent speeds, and with thinner plates, the flux of heat from within the slab has time to penetrate to the surface of the slab, contributing to its warming, so that the temperature profile is smoother.

The majority of solutions show a smooth temperature increase, and we obtain an expression for the perturbation to heat flux out of the slab in this case by treating the slab as a semi-infinite medium whose surface is kept at a temperature

$$T(0, t) = Ct^{m/2}, \tag{A30}$$

where t is time since the top of the slab passed beneath the Earth's surface and C is a constant. The perturbation to the temperature gradient at the top of the slab caused by this boundary condition is, for m a positive integer,

$$\left. \frac{\partial T}{\partial x} \right|_{x=0} = b \frac{T(0, t)}{\sqrt{\kappa t}}, \tag{A31}$$

where (Carslaw & Jaeger 1959, p. 63)

$$b = \frac{\Gamma(m/2 + 1)}{\Gamma(m/2 + 1/2)}. \tag{A32}$$

We let the moderate variation of surface temperature with time, seen in Fig. 5, be represented by (A30) with $m = 1$ or 2, in which case $b \sim 1$ and

$$\left. \frac{\partial T}{\partial x} \right|_{x=0} = \frac{T_s}{\beta}, \tag{A33}$$

where T_s is the temperature at the top of the slab at the depth, z, of interest and $\beta = \sqrt{\kappa t} = \sqrt{\kappa z / V \sin \delta}$.

Summing the contributions to the temperature gradient within the slab and close to its top from the decay of the original thermal profile in the slab (eqs A29 and A33) yields the heat flux out of the top of the slab:

$$Q|_- \sim K \left[\frac{T_s}{\beta} - \frac{T_a}{a} \mathrm{erf}\left(\frac{a}{2\sqrt{\kappa t}} \right) \right]. \tag{A34}$$

Hence, matching heat fluxes across the top of the slab,

$$T_s \sim \left[T_1 + \frac{\sqrt{\pi}\alpha T_a}{2a} \mathrm{erf}\left(\frac{a}{2\sqrt{\kappa t}} \right) \right] \Big/ \left(1 + \frac{\sqrt{\pi}\alpha}{2\beta} \right). \tag{A35}$$

The quality of the approximation in (A35) is assessed in Section 3.3.

For most present subduction zones, $\alpha < 20$ km and the ocean floor is 50 Myr old, or older. For these conditions, $\alpha \ll a$ and the second term in the numerator is much smaller than the first so may be neglected, yielding a simpler expression for the relation between T_s and T_1:

$$T_s \sim T_1 \left(1 + \frac{\sqrt{\pi}\alpha}{2\beta} \right)^{-1}. \tag{A36}$$

Substituting $\beta = \sqrt{\kappa z / V \sin \delta}$, and for α from (A17),

$$\frac{\sqrt{\pi}\alpha}{2\beta} = \left(\frac{2\pi}{9\xi} \right)^{1/3} \left(1 - \frac{z_w}{z} \right) \left(\frac{V\delta^2 r}{\kappa} \right)^{1/6}, \tag{A37}$$

where we have used $r = (z - z_w)/\sin \delta$. The first term on the right-hand side of (A37) is approximately 0.85 for $0 \le \delta \le \pi/2$, and the second term is close to unity for depths $z \gg z_w$. For the ranges of V, r and δ in modern subduction zones (Table 2), the quantity $V r \delta^2 / \kappa$ varies between about 50 and 200 beneath the arc volcanoes and between about 200 and 800 where the slabs reach depths of 400 km. The range in the one-sixth power of this quantity is from 1.9–3, and the denominator in (A35) ranges from about 2.6 to 3.6 for depths $z \gg z_w$.

A4 Maximum temperature in the wedge

We obtain an expression for the maximum temperature, T_1, in the wedge at any radial distance, r, from the wedge corner by considering the balance of heat fluxes across an annular segment of wedge, $0 \le \theta \le \delta$. We may neglect the radial diffusion of heat in comparison with the radial advection of heat, and write the total rate of heat transport in the radial direction as

$$-\rho c r \int_0^\delta u_r \frac{\partial T}{\partial r} d\theta, \tag{A38}$$

where ρ is density and c is specific heat. We distinguish three regimes of advection within the wedge. Near the upper boundary, the velocities are much slower than elsewhere in the wedge (Fig. 1), and we neglect advection here. At the top of the slab there is an advective boundary layer, of thickness α and of average temperature $(T_1 + T_s)/2$; we approximate the radial component of velocity, u_r, in this layer by the speed, V, of the slab. The volume flux, per unit length, in the advective boundary layer in the radial direction is, by this approximation, $V\alpha$, and the contribution to (A38) from this layer is

$$-\rho c V \alpha \frac{d}{dr}\left(\frac{T_1 + T_s}{2}\right). \tag{A39}$$

The volume flux, per unit length, through the wedge above the advective boundary layer on top of the slab must, by conservation of mass, be $-V\alpha$ and we assume that all significant advection of heat in this part of the wedge takes place in the isothermal core of the wedge, at its temperature T_1. The contribution to (A38) from this part of the wedge is

$$\rho c V \alpha \frac{dT_1}{dr}. \tag{A40}$$

The advection of heat towards the corner is balanced by diffusion of heat into the slab and the overriding plate. Because the temperature gradients above the slab are generally much greater than the temperature gradients at the base of the overriding plate (see, for example, Fig. 1), we neglect diffusive heat loss into the overriding plate. Substituting (A39) and (A40) into (A38) and equating to this advective flux to the diffusive loss into the slab, given by (A25), we obtain

$$\frac{\rho c V \alpha}{2}\frac{d(T_1 - T_s)}{dr} = \frac{2K(T_1 - T_s)}{\sqrt{\pi}\alpha}. \tag{A41}$$

The discussion at the end of the previous subsection shows that, for fixed V, δ, the ratio of T_s to T_1 varies as the one-sixth power of r, thus we may make the approximation that T_s is a constant fraction of T_1 at all depths, hence

$$\frac{\rho c V \alpha}{4}\frac{dT_1}{dr} = \frac{K T_1}{\sqrt{\pi}\alpha}. \tag{A42}$$

Substituting for α from (A17) into (A42) we obtain

$$\frac{1}{T_1}\frac{dT_1}{dr} = \gamma r^{-4/3}, \tag{A43}$$

where

$$\gamma = \left(\frac{81\xi^2}{4\sqrt{\pi}}\right)^{1/3}\left(\frac{\kappa}{V\delta^2}\right)^{1/3}.$$

This gives

$$T_1 = A\exp\left(-3\gamma r^{-\frac{1}{3}}\right). \tag{A44}$$

We note (Fig. 1) that the maximum temperature in the wedge is reached where $\theta \sim 2\delta/3$, equivalent to $\phi \sim \delta/3$. We may evaluate A by identifying the radial position, R, at which the advective boundary layer on top of the slab is first thinner than $r\delta/3$. Below this radius, the boundary layer on top of the slab is connected to that beneath the overriding plate, and T_1 increases with distance from the wedge corner; above this radius, the boundary layers are separated by the isothermal core of the wedge, and $T_1 = T_a$. The temperature in the advective boundary layer on top of the slab (A18) approaches T_1 to within 1 per cent when $x \sim 2\alpha$, thus the critical radius, R, is given by $(R\delta/3) \sim 2\alpha$, or

$$R \sim \frac{6\alpha}{\delta} = \left(\frac{384\kappa R^2}{\sqrt{\pi}\xi V\delta^2}\right)^{1/3}$$

$$R = \frac{384\kappa}{\sqrt{\pi}\xi V\delta^2}. \tag{A45}$$

We thus obtain

$$T_1 = T_a\exp\left[3\gamma(R^{-1/3} - r^{-1/3})\right]$$

$$= T_a\exp\left\{\frac{9\xi}{8}\left[1 - \left(\frac{R}{r}\right)^{1/3}\right]\right\} \quad 0 < r < R$$

$$= T_a \quad r \geq R. \tag{A46}$$

The form of (A46) is more complicated than is warranted by the level of approximation we have made. Recognizing that ξ varies little, and is close to 0.5 (eq. A4 and following) we employ a simplified version of this expression to approximate the maximum temperature in the wedge:

$$T_1 \sim T_a\exp\left\{\frac{1}{2}\left[1 - \left(\frac{R}{r}\right)^{1/3}\right]\right\} \quad 0 < r < R,$$

$$= T_a \quad r \geq R, \tag{A47}$$

with $R = 400\kappa/V\delta^2$. The quality of this approximation is assessed in Section 3.2.